

# Molecular Engineering of an Alkaline Naphthoquinone Flow Battery

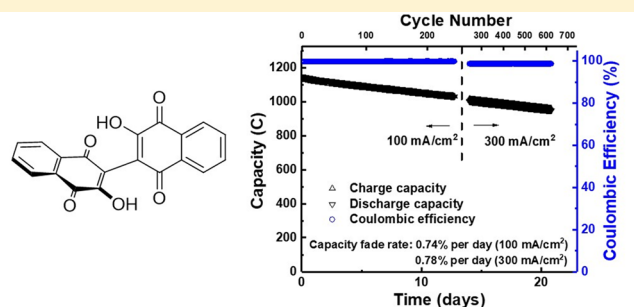
Liuchuan Tong,<sup>†</sup> Marc-Antoni Goulet,<sup>‡,§</sup> Daniel P. Tabor,<sup>†</sup> Emily F. Kerr,<sup>†</sup> Diana De Porcellinis,<sup>‡</sup> Eric M. Fell,<sup>‡</sup> Alán Aspuru-Guzik,<sup>†,⊥</sup> Roy G. Gordon,<sup>\*,†</sup> and Michael J. Aziz<sup>\*,‡,⊥</sup>

<sup>†</sup>Department of Chemistry and Chemical Biology, Harvard University, 12 Oxford Street, Cambridge, Massachusetts 02138, United States

<sup>‡</sup>John A. Paulson School of Engineering and Applied Sciences, Harvard University, 29 Oxford Street, Cambridge, Massachusetts 02138, United States

## Supporting Information

**ABSTRACT:** Aqueous organic redox flow batteries (AORFBs) have recently gained significant attention as a potential candidate for grid-scale electrical energy storage. Successful implementation of this technology will require redox-active organic molecules with many desired properties. Here we introduce a naphthoquinone dimer, bislawsonone, as the redox-active material in a negative potential electrolyte (negolyte) for an AORFB. This dimerization strategy substantially improves the performance of the electrolyte versus that of the lawsone monomer in terms of solubility, stability, reversible capacity, permeability, and cell voltage. An AORFB pairing bislawsonone with a ferri/ferrocyanide positive electrolyte delivers an open-circuit voltage of 1.05 V and cycles at a current density of 300 mA/cm<sup>2</sup> with a negolyte concentration of 2 M electrons in alkaline solution. We determined the degradation mechanism for the naphthoquinone-based electrolyte using chemical analysis and predicted theoretically electrolytes based on naphthoquinones that will be even more stable.



Naphthoquinone Dimer for Improved Flow Battery Performance

The cost of renewable solar and wind electricity has dropped so much that the greatest barrier to their widespread adoption is their intrinsic intermittency. A cost-effective, long discharge duration electrical energy storage solution could solve the problem of unbalanced supply and demand. Among the various proposed technologies, redox-flow batteries<sup>1</sup> are particularly attractive for long discharge duration because liquid redox-active electrolytes can be stored in external tanks that are separated from the power generating stack. With this design, energy capacity can be scaled independently of power capacity by simply changing the volume of electrolyte.

Recent years have seen a great deal of research into developing organic redox-active species for aqueous flow battery electrolytes. These redox-active materials are based on earth-abundant elements such as carbon, nitrogen, oxygen, and sulfur and usually utilize well-known redox-active compounds such as quinones,<sup>2–9</sup> viologens,<sup>10–13</sup> ferrocenes,<sup>14,15</sup> azaromatics,<sup>16–18</sup> and nitroxide radicals.<sup>10,11,19</sup> Organic-based aqueous flow batteries offer several advantages over vanadium and nonaqueous-based flow batteries in cost, scalability, and safety. In addition, the use of organic molecules in flow batteries opens a vast chemical space for tailoring the properties of redox-active electrolytes, including solubility,

reduction potential, rate capacity, and stability. Within the quinone family, benzoquinones<sup>6</sup> and anthraquinones<sup>2,4,7,9</sup> have been explored extensively as redox-active electrolytes in aqueous organic flow batteries. To date, however, there are limited reports on using naphthoquinone as an active electrolyte not only because of stability and solubility concerns but also because naphthoquinone reduction potentials tend to be intermediate between those of benzoquinones and anthraquinones, making them unsuitable for either terminal of an aqueous flow battery. 2-Hydroxynaphthoquinone, commonly known as lawsone, is a natural product extracted from the leaves of the henna plant and the flower of the water hyacinth, which makes its use or derivatives of it particularly appealing from a cost and scalability perspective.<sup>20</sup> Lawsone has been explored as a candidate for alkaline flow batteries;<sup>21,22</sup> however, poor cycling stability has limited further investigation into this class of molecules. It is hypothesized that the C–H position next to the quinone functional group in the molecule is prone to Michael addition, particularly in alkaline media, and

Received: June 19, 2019

Accepted: July 11, 2019

Published: July 11, 2019

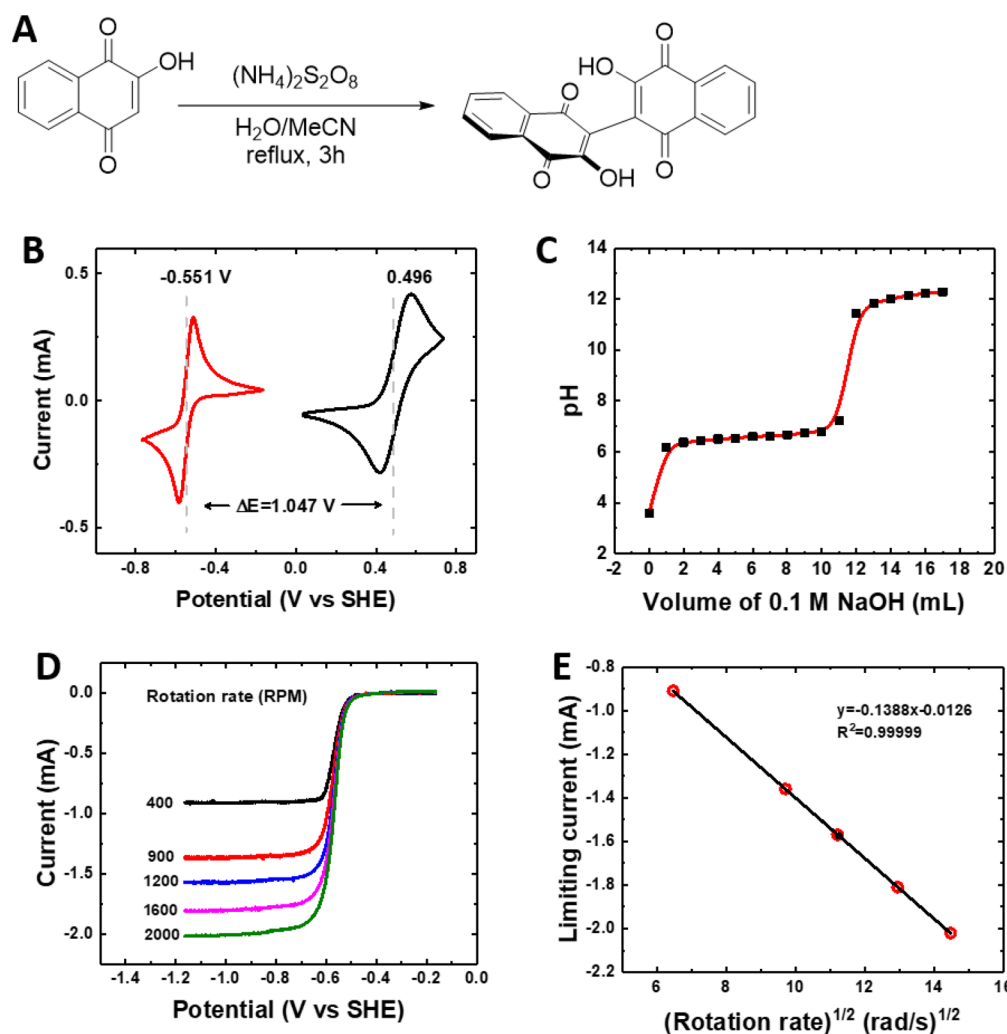


**Figure 1.** Synthesis and physical characterization of bislawsone. (A) Synthetic scheme of bislawsone. (B) Cyclic voltammograms of 5 mM bislawsone (red) and 10 mM potassium ferrocyanide (black) in 1 M KOH at a scan rate of 50 mV/s. The redox potential vs SHE is indicated. (C) Titration of 10 mL of 0.05 M bislawsone using 0.1 M NaOH solution. (D) Rotating disk electrode (RDE) measurements of bislawsone using a glassy carbon electrode in 1 M KOH at 5 rotation rates. (E) Levich plot of limiting current versus square root of rotation rate ( $\omega^{1/2}$ ).

subsequent degradation from hydroxide or other nucleophiles during cycling.<sup>6,23,24</sup> Efforts to modify the molecule have been made by installing a carboxyl group onto the open aromatic C–H position. Despite the increased solubility of this derivative, capacity utilization, cycling stability, and permeability remain as issues.<sup>25</sup>

Here, we report a naphthoquinone dimer 2,2'-bis(3-hydroxy-1,4-naphthoquinone), or bislawsone, as a high-capacity, reversible negolyte material for aqueous organic flow batteries. Bislawsone was constructed by taking advantage of the reactive open site and linking two lawsone units via their 3-position. We demonstrate that this dimerization strategy improves solubility, stability, reduction potential, and permeability without compromising the capacity per molecular weight. We also elucidate the degradation mechanism of bislawsone and propose strategies to further stabilize the molecule based on theoretical calculations. We draw important implications for the synthetic strategy and rational design of stable quinone molecules for AORFBs.

**Synthesis and Physical Properties Study.** Bislawsone was synthesized via a one-step radical dimerization of the natural product lawsone using inexpensive chemicals and solvents

(Figures 1A, S1, and S2). No further steps were necessary to purify this yellow powder. Its physical and electrochemical properties were evaluated. Cyclic voltammetry of bislawsone in 1 M KOH showed a reduction potential of  $-0.551$  V vs standard hydrogen electrode (SHE) with a peak separation ( $\Delta E$ ) of 71 mV for 4 electrons. The reduction potential is 50 mV more negative than that of the lawsone monomer with overlapping peaks for the two subunits (Figure S3A), indicating higher cell voltage, and improved reversibility despite the doubling of the molecular size and the number of electrons transferred. Pairing this electrolyte with potassium ferrocyanide should yield an equilibrium cell potential of 1.05 V (Figure 1B). Considering the sharpness of the CV peaks, the two redox centers in the molecule do not appear to interact with each other; this conclusion is also supported by theoretical calculations (Figure 4). The  $pK_a$  values ( $\sim 6.5$ ) for each of the hydroxyl groups in the molecule are indistinguishable by titration and are slightly higher than that of lawsone (Figures 1C and S3B and Table S1). The two low- $pK_a$  phenols in bislawsone serve as the solubilizing groups in alkaline solution. To our surprise, the solubility of bislawsone reached 0.56 M (2.24 M electrons or 60.0 Ah/L) in pH 14

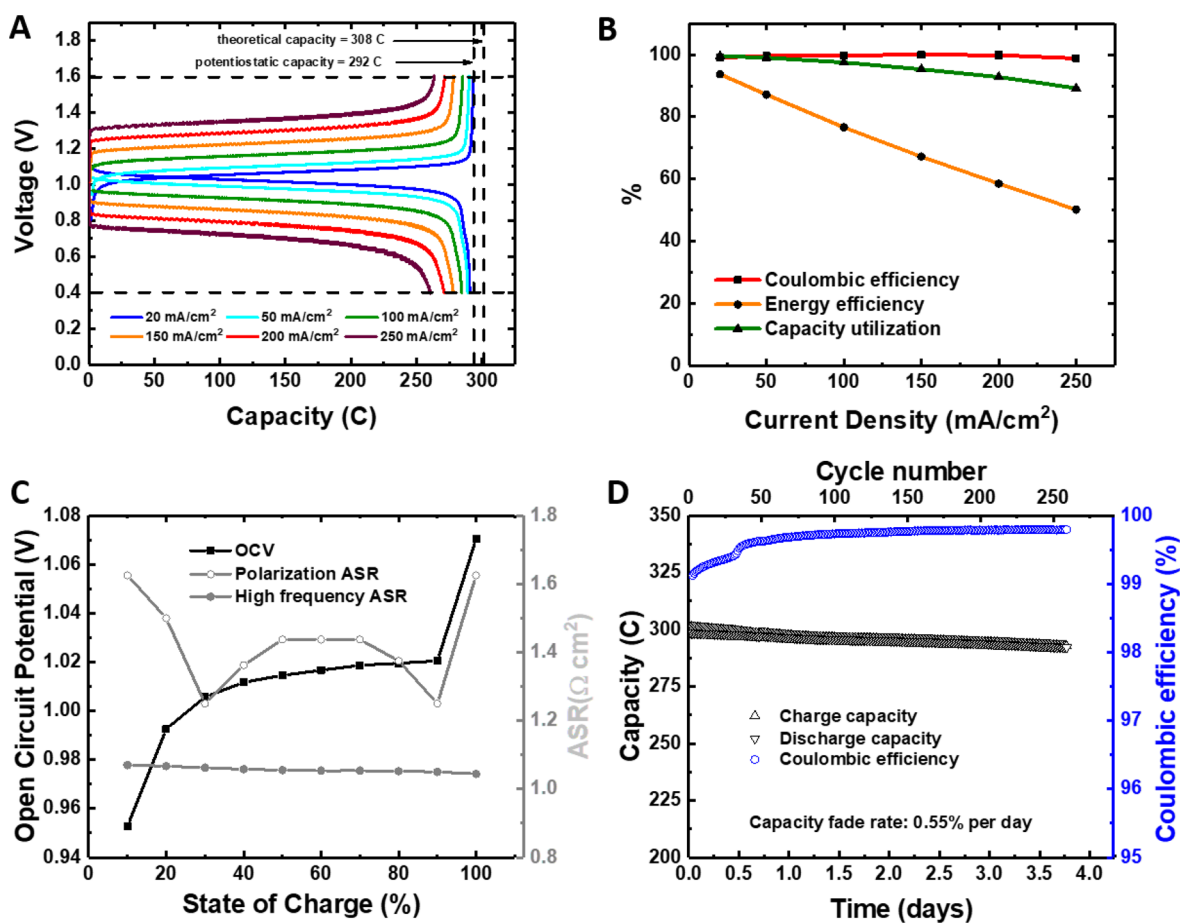


Figure 2. Full cell characterization of low-concentration 0.1 M bislawsone. The negolyte comprised 8 mL of 0.1 M bislawsone in 1 M KOH while, the nonlimiting posolyte comprised 45 mL of 0.2 M potassium ferrocyanide and 0.02 M potassium ferricyanide in 1 M KOH solution. (A) Galvanostatic charge and discharge curves from 20 to 250 mA/cm<sup>2</sup>. The vertical dashed lines indicate the maximum capacity realized with potentiostatic charge and discharge at the voltage cutoffs (1.6 and 0.4 V, respectively), as well as the theoretical capacity. (B) Coulombic efficiency, round-trip energy efficiency, and capacity utilization as a percentage of potentiostatic capacity versus current density. (C) OCV, high-frequency ASR, and polarization ASR versus SOC. (D) Coulombic efficiency (circles) and charge (upward-pointing triangles) and discharge (downward-pointing triangles) capacity versus time and cycle number for a negolyte-limited bislawsone cell. The cell was cycled galvanostatically at 100 mA/cm<sup>2</sup> for 3.8 days. The cell was cycled between 1.4 and 0.5 V, and each half cycle ended with a potentiostatic hold until the magnitude of the current density fell below 2 mA/cm<sup>2</sup>.

solution, as compared to the 0.48 M (0.96 M electrons) solubility of lawsone in pH 14 solution. The origin of this increased solubility is hypothesized to be from the nonplanar nature of the dimer along the 3,3'-single bond. The nonplanar feature may disrupt crystal packing, which would raise the solubility of the whole molecule compared to that of the planar monomer. The increased solubility of the dimer is in contrast with the usually decreased solubility of many extended polymers compared to their parent monomers.<sup>26</sup>

A dimerization strategy, as employed in the case of bislawsone, should offer the advantage of lowered permeability without significantly compromising the diffusivity or viscosity. The diffusion coefficient ( $D$ ) of bislawsone was determined by rotating disk electrode measurement and calculated according to the Levich plot of limiting current versus square root of rotation rate to be  $4.54 \times 10^{-6}$  cm<sup>2</sup>/s (Figure 1D,E), which is in line with those of most small organic molecules.<sup>2,4,6,9,25</sup> The viscosity of bislawsone dissolved in 1 M KOH was consistently below 2 cP for concentrations up to the solubility limit (Figure S4), which bodes well for minimizing energy inefficiency due to pumping loss. The crossover rates of bislawsone and lawsone through a Fumasep E-620 K cation exchange

membrane were measured in a two-compartment rotating cell (Figure S5). The permeability of bislawsone was determined to be  $1.19 \times 10^{-11}$  cm<sup>2</sup>/s, which is an order of magnitude lower than the value of  $1.01 \times 10^{-10}$  cm<sup>2</sup>/s for lawsone, as expected.

**Electrochemical and Full Cell Study.** We assembled an alkaline flow battery with a positive electrolyte (posolyte) comprising 44 mL of 0.2 M potassium ferrocyanide and 0.02 M potassium ferricyanide and a negative electrolyte (negolyte) comprising 8 mL of 0.1 M (0.4 M electrons) bislawsone in 1 M KOH solution (see "Full Cell Measurement" in the Supporting Information), separated by a Fumasep E620 K cation-exchange membrane. This nonfluorinated membrane has been shown to provide very low permeability to ferro/ferricyanide and to anthraquinones.<sup>9</sup> These solutions were pumped through a flow cell constructed from graphite flow plates and carbon paper electrodes. During charging, the negolyte biquinone was reduced into bihydroquinone while the ferrocyanide was oxidized into ferricyanide. An excess amount of ferrocyanide was used in the cell testing in order to isolate the negolyte as the capacity-limiting side.

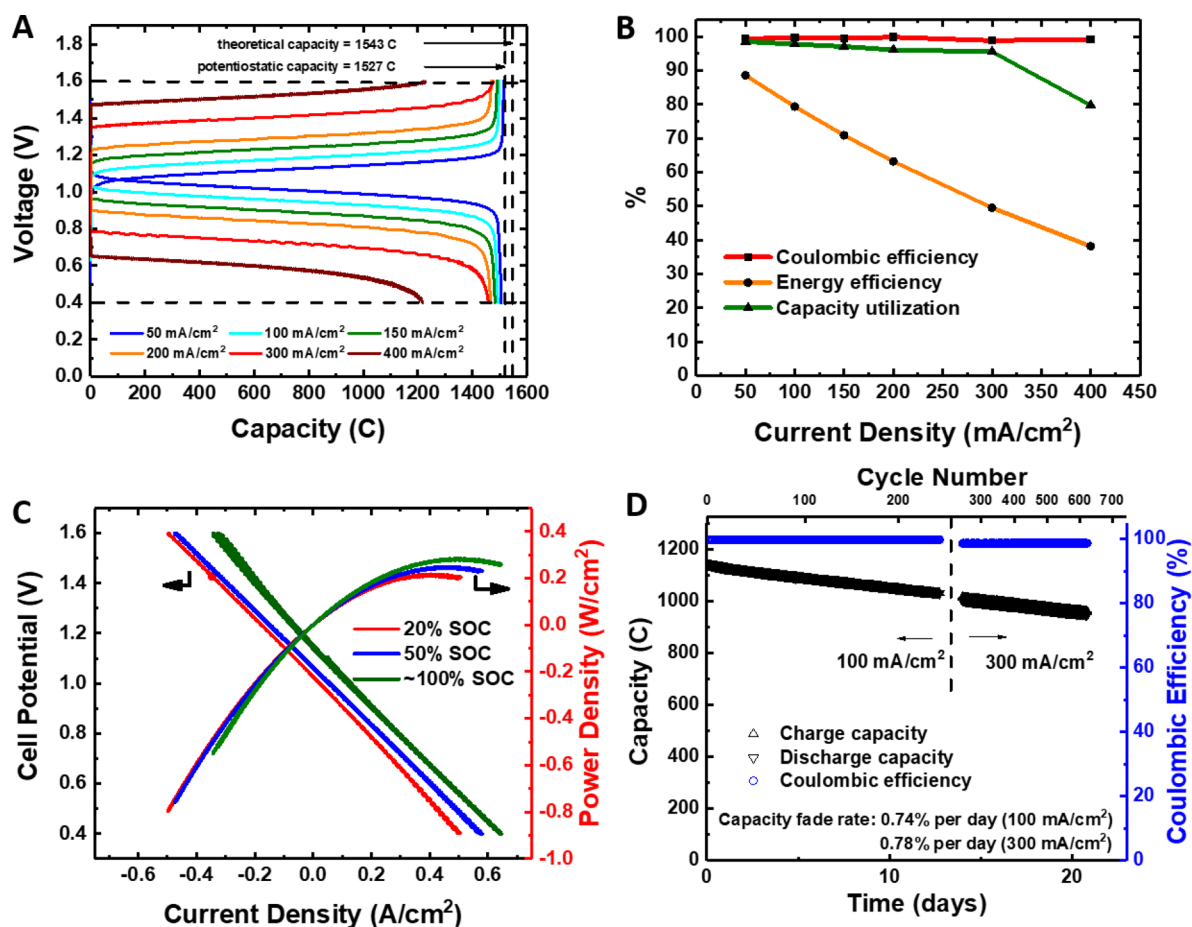


Figure 3. Full cell characterization of high-concentration 0.5 M bislawsonone. The negolyte comprised 8 mL of 0.5 M bislawsonone in 1 M KOH, while the nonlimiting posolyte comprised 95 mL of 0.3 M potassium ferrocyanide and 0.1 M potassium ferricyanide in 1 M KOH solution. (A) Galvanostatic charge–discharge voltage profiles from 50 to 400 mA/cm<sup>2</sup>. The vertical dashed lines indicate the maximum capacity realized with potentiostatic charge and discharge at the voltage cutoffs (1.6 and 0.4 V, respectively), as well as the theoretical capacity. (B) Coulombic efficiency, round-trip energy efficiency, and capacity utilization as a percentage of potentiostatic capacity versus current density. (C) Cell voltage versus discharge current density at room temperature at 20%, 50%, and 100% SOC. (D) Coulombic efficiency (circles), charge (upward-pointing triangles), and discharge (downward pointing triangles) capacity versus time and cycle number for a negolyte-limited bislawsonone cell. The cell was cycled galvanostatically at 100 mA/cm<sup>2</sup> for 12.8 days and then rested for 1.2 days before switching to 300 mA/cm<sup>2</sup> for 6.8 days. The cell was cycled between 1.4 and 0.5 V, and each half cycle ended with a potentiostatic hold until the magnitude of the current density fell below 2 mA/cm<sup>2</sup>. The volume of negolyte with same composition used was 6 mL in panel D.

To confirm that all four electrons in bislawsonone can be accessed reversibly, the cell was cycled at different current densities ranging from 20 to 250 mA/cm<sup>2</sup> (Figure 2A). For each current density tested, a > 99% Coulombic efficiency and >90% capacity utilization were achieved based on the four-electron experimental potentiostatic capacity. A capacity utilization of 97.5% and round-trip energy efficiency of 77% was reached at 100 mA/cm<sup>2</sup> (Figure 2B). The nuclear magnetic resonance (NMR) spectrum of a charged negolyte showed a clean conversion to the fully reduced bislawsonone (Figure S6). The high-capacity utilization at high current density demonstrated that the dimerization strategy does not negatively affect the kinetics and accessed capacity.

A charging current of 100 mA/cm<sup>2</sup> was applied to charge the cell, and polarization curves were measured at 20, 50, and 100% states of quinone charge (SOC). The open-circuit voltage (OCV) is 1.01 V at 50% SOC and 1.07 V at 100% SOC (Figure 2C), consistent with CV measurement. The membrane resistance contributed the largest fraction of the overall resistance; it can possibly be decreased in the future by manipulating the electrolyte composition and by decreasing

the membrane thickness. The polarization curve (Figure S7) shows no sign of redox kinetic limitations and exhibits a peak galvanic power density exceeding 0.20 W cm<sup>-2</sup>.

The viability of a flow battery hinges on the long-term stability of the system. Molecular stability has been a major concern for organic-based flow battery systems as there are many potential degradation pathways for organic molecules. Capacity fade may have both temporal or electrochemical cycling contributions, with the former dominating the lifetimes of the organic molecules that have been carefully studied to date.<sup>27</sup> To investigate the long-term stability of bislawsonone, prolonged galvanostatic cycling of the 0.1 M bislawsonone cell was performed at 100 mA/cm<sup>2</sup> (Figure 2D). In order to avoid temporal variations in accessed capacity and to ensure that 100% of the redox-active material was cycled, potential holds at 1.4 and 0.5 V were applied until the magnitude of the current density fell below 2 mA/cm<sup>2</sup>. 95% of theoretical capacity was accessed. The 5% discrepancy may be due to material transfer and residual water in the synthesized bislawsonone powder. Over a 3.8 day period of cycling, a 2% capacity loss was observed, which corresponds to a capacity fade rate of 0.55% per day, or



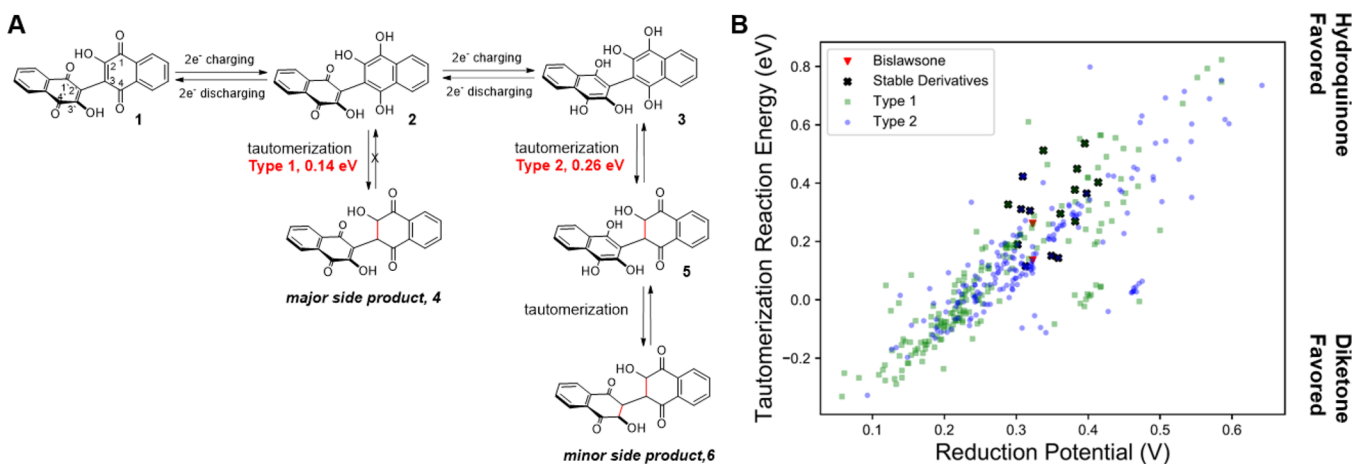


**Figure 4.** Decomposition study and theoretical calculations. (A) Scheme of decomposition pathway. The red text shows the calculated reaction energies of the reduced forms tautomerizing as calculated at the B3LYP/6-311+G(d,p) (PCM) level of theory (indicated reaction energy is the tautomerization side product ground-state energy – the reduced form ground-state energy). (B) Calculated tautomerization reaction energies plotted against calculated reduction potential of the couple. Type 1 and type 2 refer to the nature of the intermediate: a “half-reduced” molecule (type 1) or a fully reduced molecule (type 2). Bislawsonone is labeled with red triangles, and eight stable derivatives within 0.1 V of the bislawsonone reduction potential are labeled with black x’s.

0.008% per cycle. The cell maintained an average of 99.5% Coulombic efficiency, and membrane resistance remained unchanged before and after the cycling. The capacity fade rate indicates that the lifetime is approximately an order of magnitude longer than that of unprotected lawsone,<sup>21,22</sup> demonstrating the protective effect of the dimerization strategy employed.

To investigate the performance at high concentration, a 0.5 M bislawsonone cell (2 M electrons, 53.6 Ah/L) was constructed. All four electrons per molecule were accessed at high concentration, as shown in Figure 3A, leading to a 95.5% capacity utilization even at 300 mA cm<sup>-2</sup> (Figure 3B). This near-quantitative capacity utilization at high current density has not been reported before to our knowledge in alkaline organic flow battery systems, which are usually limited by cell resistance and molecular diffusion. At 400 mA/cm<sup>2</sup>, a lower capacity (80.0%) was accessed because membrane resistance dominated the voltage profile and the cell voltage quickly reached the 1.6 and 0.4 V voltage cutoffs. At 100 mA/cm<sup>2</sup>, 97.7% of the capacity was reversibly accessed with a Coulombic efficiency of 99.7% and round-trip energy efficiency of 79.3%, representing a significant improvement over a lawsone flow battery which had 70% accessed capacity and 68% round-trip energy efficiency.<sup>25</sup> The OCV of the 0.5 M bislawsonone cell displayed typical Nernstian behavior with respect to SOC (Figure S8). A peak galvanic power density of 0.28 W/cm<sup>2</sup> was achieved as determined by the polarization curve at near 100% SOC (Figure 3C). The power density is mainly limited by high-frequency area-specific resistance. This is dominated by the membrane resistance (Figure S8), which is above 1 Ω·cm<sup>2</sup>; it can possibly be decreased in the future by manipulating the electrolyte composition and by using a membrane with better conductivity.

Long-term galvanostatic cycling of the 0.5 M bislawsonone cell was performed at 100 mA cm<sup>-2</sup> with potential holds at 1.4 V for charging and 0.5 V for discharging until the current density dropped to 2 mA/cm<sup>2</sup> (Figure 3D). 98.3% of the theoretical capacity was accessed. After 12.8 days of cycling, the capacity had faded by 9.5%, which corresponds to a temporal capacity fade of 0.74% per day, or 0.038% per cycle. Because excess

amounts of polysolite ferrocyanide and ferricyanide were used in the cycling, we attribute the slow capacity fade to the bislawsonone negolyte. The per cycle capacity fade in the high-concentration cell was superficially higher compared to the low-concentration cell because of longer per cycle cycling time in the high-concentration cell. The per day capacity fade rate is similar to that of the low-concentration cell (0.74% vs 0.55% per day), indicating that the stability of bislawsonone is time-dependent rather than cycle-dependent.

Encouraged by our high capacity utilization at high current density, we cycled the 0.5 M bislawsonone cell at a higher current density of 300 mA/cm<sup>2</sup>. The cell maintained high capacity rate and stable charging/discharging plateau during the 6.8 days of continuous cycling with 98.8% Coulombic efficiency. The cell lost 5.3% of its capacity, which corresponds to 0.78% loss per day. This rate is almost identical to the 0.74%/day loss rate when cycled at 100 mA/cm<sup>2</sup>, demonstrating that bislawsonone can be cycled at high current density under alkaline conditions without compromising its stability.

*Investigation and Potential Mitigation of Chemical Degradation.* Different strategies have been used in the field to synthesize more stable derivatives based on various redox-active scaffolds. However, the chemical space available for organic molecules is huge. Therefore, it is important to understand how a scaffold molecule degrades in order to rationally design the next generation of molecules with better performance. Despite the fact that bislawsonone can inhibit Michael-addition decomposition pathway as compared to lawsone, capacity loss in our system was still observed. We have recently elucidated the molecular degradation mechanism of anthraquinones in flow batteries using 2,6-dihydroxyanthraquinone as a model system.<sup>27</sup> We therefore studied the degradation of naphthoquinones using bislawsonone as a model system. A sample was taken from the above cycled discharged 0.5 M cell and subjected to NMR analysis. One major side product was observed which accounts for 14.2% of the total NMR active material (Figure S9). High-resolution liquid chromatography mass spectrometry (LC-MS) analysis found only one major side product with the mass-to-charge ratio of 347.0559 in negative ionization mode (Figure S10). Back

calculation of the neutral mass gives  $C_{20}H_{12}O_6$  as the molecular formula, which coincides in mass with a partial (2-electron) reduction of bislawsone starting material  $C_{20}H_{10}O_6$ .

In order to elucidate the chemical structure, the degradation product was isolated by preparative-scale high-performance liquid chromatography (pHPLC, Figure S11).  $^1H$ ,  $^{13}C$ , and 2D NMR analysis on the purified degradation product showed the asymmetry between two monomer units, and the presence of two aliphatic proton peaks with doublet splitting patterns (Figures S12–S14) indicated a disruption in the conjugated system. Together, the NMR and LC-MS analyses are consistent with the structure where the bond between C2 and C3 of the bislawsone is reduced to a carbon–carbon single bond, locking the quinone unit into a diketone molecule, 2,3-dihydrobislawsone 4 (Figure 4A, type 1 tautomerization). Electrochemical reduction of a ketone into an alcohol and reoxidation of the alcohol back to the ketone have high overpotentials and usually require a metal or organic catalyst;<sup>28–31</sup> therefore, this side product should generally be considered as redox-inactive in a catalyst-free flow battery system using a carbon-based electrode. Because the similar degradation rate suggests a concentration and rate-independent degradation mechanism, the production of 2,3-dihydrobislawsone is not due to the direct reduction or oxidization by the electrode, but rather by the enol-ketone tautomerization of the partially reduced quinone-hydroquinone molecule, which is a process governed by kinetics and thermal equilibrium. The degradation of bislawsone into 2,3-dihydrobislawsone may be a general degradation mechanism for naphthoquinones. This conclusion is backed by some earlier studies,<sup>32,33</sup> which documented the tautomerization of reduced naphthoquinone. While this tautomerization was observed in many different naphthoquinone derivatives in earlier studies, the equilibrium and kinetics were heavily influenced by the substitution groups on the naphthoquinone ring. In this work, the 2,3-dihydrobislawsone did not tautomerize back to the half-reduced hydroquinone form 2, as the isolated 2,3-dihydrobislawsone was stable in air and alkaline solution. Given this general phenomenon, we expect that the tautomerization should also occur for the fully reduced bislawsone 3 at a different rate (Figure 4A, type 2), which can eventually result in a 4-electron reduction 2,2',3,3'-tetrahydrobislawsone form 6 (tetra-ketone instead of biquinone) that is completely redox inactive. Indeed, careful LC-MS analysis of a discharged sample also found a molecule at a much lower concentration with an atomic mass that corresponds to a 4-electron reduction product after cycling (Figure S15). This molecule cannot be fully reduced bislawsone 3 because the sample was taken at the fully discharged state and exposed to air prior to analysis and therefore is expected to be the redox-inactive tetra-ketone form.

Based on the structure of the degradation product, the degradation of bislawsone into the diketone form 4 should disrupt only half of the redox activity, as the other lawsone monomer unit stayed intact. Therefore, 2,3-dihydrobislawsone 4, which accounts for 14.2% of total NMR-active material, should impact only 7.1% of the total capacity. However, 14.8% of the capacity was lost in 21 days of cycling. There are several possibilities to account for the 7.7% difference. First, once reduced naphthoquinone 2 tautomerized into diketone form 4, the 2-hydroxy group changed from a low- $pK_a$  phenol group into a high- $pK_a$  alcohol group and would stay protonated in alkaline solution. Therefore, the solubility of the 2,3-

dihydrobislawsone molecule is expected to drop drastically and precipitate out of the solution, making it practically redox-inactive. A precipitate was indeed observed in the electrolyte that has been cycled for a long time. Second, the tetra-ketone form, 2,2',3,3'-tetrahydrobislawsone 6, accounts for 1% of the degradation product as detected by LC-MS; however, its concentration is too low to be detected in NMR, and it is expected to have even lower solubility due to the transformation of two solubilizing phenol groups into two alcohol groups. Other minor degradation products or NMR silent species and cell leakage may also contribute to the remaining capacity fade.

The equilibrium of hydroquinone-diketone is heavily influenced by the substituents on the naphthoquinone core; therefore, this presents an opportunity for a next-generation naphthoquinone with a rationally designed substituent group. We have calculated (see the Theoretical Calculation section in the Supporting Information) the stability and reduction potentials of 637 lawsone redox couples, which include 193 bislawsone derivatives. Figure 4B shows the correlation between the tautomer reaction energies and the predicted standard reduction potentials of redox couples. In general, lower reduction potentials are more likely to be subject to tautomerization than higher reduction potentials. Interestingly, despite the fact that the predicted standard reduction potentials of each of the two reductions of bislawsone are within 0.01 V of each other, the “type 1” decomposition is more thermodynamically favored than the “type 2” decomposition.

Of these, we predict that 8 bislawsone derivatives with reduction potentials within 0.1 V of bislawsone potentially have higher stability than bislawsone (Figure S16). One common motif in these stabilized molecules are oxy-alkyl substitutions, which have previously been shown to stabilize anthraquinone molecules against other decomposition mechanisms.<sup>9</sup> Our calculations also indicate that the increased stability of bislawsone can be at least partially attributed to its protection against a tautomerization reaction relative to lawsone. Efforts to synthesize a more stable naphthoquinone are underway.

In summary, we demonstrate that dimerization is a promising synthetic strategy to improve the performance of quinone-based flow batteries. The bislawsone flow battery reported in this work delivered a high negolyte volumetric capacity, theoretically 53.6 Ah/L (2 M electrons), with peak power density of 0.28 W/cm<sup>2</sup>. It reversibly accessed >95.5% of theoretical capacity at a current density of 300 mA/cm<sup>2</sup> with significantly improved permeability and stability, making naphthoquinone a more practical redox-active negolyte in AORFBs. We identified tautomerization of the reduced naphthoquinone to the redox-inactive ketone form as a degradation mechanism of naphthoquinone in flow batteries. This mechanistic insight allowed us to propose more stable naphthoquinones and rationally design next-generation organics for AORFB which could accelerate the use of wind and photovoltaic electricity.

## ■ ASSOCIATED CONTENT

### Supporting Information

The Supporting Information is available free of charge on the ACS Publications website at DOI: 10.1021/acseenergylett.9b01321.

Details of cell assembly, electrochemical characterization, theoretical calculation, and other results, including NMR spectra, LC-MS, and a Frequently Asked Questions section (PDF)

Energies (B3LYP/6-311+G(d,p) PCM) of eight predicted stable molecules (XLSX)

Energies of all the molecules in the full library (XLSX)

## AUTHOR INFORMATION

### Corresponding Authors

\*Roy G. Gordon: Dept. of Chemistry and Chemical Biology, Harvard University, 12 Oxford Street, MA 02138. Tel: +1 617-495-4017. Fax: +1 617-495-4723. E-mail: [Gordon@chemistry.harvard.edu](mailto:Gordon@chemistry.harvard.edu).

\*Michael J. Aziz: John A. Paulson School of Engineering and Applied Sciences, Harvard University, Pierce Hall 204a, 29 Oxford Street, MA 02138. Tel: +1 (617) 495-9884. E-mail: [maziz@harvard.edu](mailto:maziz@harvard.edu).

### ORCID

Liuchuan Tong: 0000-0001-6211-6322

Daniel P. Tabor: 0000-0002-8680-6667

Alán Aspuru-Guzik: 0000-0002-8277-4434

Roy G. Gordon: 0000-0001-5980-268X

Michael J. Aziz: 0000-0001-9657-9456

### Present Addresses

<sup>§</sup>M.-A.G.: Form Energy Inc., Somerville, Massachusetts 02143, United States

<sup>†</sup>A.A.-G.: Department of Chemistry and Department of Computer Science, Vector Institute for Artificial Intelligence, University of Toronto, Toronto, Ontario, M5S 1A1, Canada.

### Author Contributions

L.T. conceived the idea, developed the synthesis, and performed molecular characterization. E.M.F. and L.T. performed rotating disk electrode characterization. E.F.K. performed additional synthesis and measured solubility and viscosity. D.D.P. performed permeability measurements. D.P.T. developed the molecular library and performed the theoretical stability calculations. Cell performance and electrolyte analysis were performed by L.T. and M.-A.G. The chemical degradation study was performed by L.T. The manuscript was drafted by L.T. and D.P.T. and revised by all authors. R.G.G. and M.J.A. supervised the experimental research, and A.A.-G. supervised the theoretical research.

### Notes

The authors declare no competing financial interest.

## ACKNOWLEDGMENTS

This work was supported in part by the following organizations: the U.S. Department of Energy Contract No. DE-AC05-76RL01830 through PNNL Subcontract No. 428977, Innovation Fund Denmark via the Grand Solutions project "ORBATS" file no. 7046-00018B, and the Massachusetts Clean Energy Technology Center. The authors thank Dr. David Kwabi and Shijian Jin for assistance and helpful discussions on experimental techniques.

## REFERENCES

- (1) Dunn, B.; Kamath, H.; Tarascon, J.-M. Electrical Energy Storage for the Grid: A Battery of Choices. *Science* **2011**, *334* (6058), 928.
- (2) Huskinson, B.; Marshak, M. P.; Suh, C.; Er, S.; Gerhardt, M. R.; Galvin, C. J.; Chen, X.; Aspuru-Guzik, A.; Gordon, R. G.; Aziz, M. J. A

metal-free organic-inorganic aqueous flow battery. *Nature* **2014**, *505* (7482), 195.

(3) Yang, B.; Hooper-Burkhardt, L.; Wang, F.; Surya Prakash, G. K.; Narayanan, S. R. An inexpensive aqueous flow battery for large-scale electrical energy storage based on water-soluble organic redox couples. *J. Electrochem. Soc.* **2014**, *161*, A1371.

(4) Lin, K.; Chen, Q.; Gerhardt, M. R.; Tong, L.; Kim, S. B.; Eisenach, L.; Valle, A. W.; Hardee, D.; Gordon, R. G.; Aziz, M. J.; Marshak, M. P. Alkaline quinone flow battery. *Science* **2015**, *349* (6255), 1529.

(5) Yang, B.; Hooper-Burkhardt, L.; Krishnamoorthy, S.; Murali, A.; Prakash, G. K. S.; Narayanan, S. R. High-Performance Aqueous Organic Flow Battery with Quinone-Based Redox Couples at Both Electrodes. *J. Electrochem. Soc.* **2016**, *163* (7), A1442.

(6) Yang, Z.; Tong, L.; Tabor, D. P.; Beh, E. S.; Goulet, M.-A.; De Porcellinis, D.; Aspuru-Guzik, A.; Gordon, R. G.; Aziz, M. J. Alkaline Benzoquinone Aqueous Flow Battery for Large-Scale Storage of Electrical Energy. *Adv. Energy Mater.* **2018**, *8*, 1702056.

(7) Gerhardt, M. R.; Tong, L.; Gómez-Bombarelli, R.; Chen, Q.; Marshak, M. P.; Galvin, C. J.; Aspuru-Guzik, A.; Gordon, R. G.; Aziz, M. J. Anthraquinone Derivatives in Aqueous Flow Batteries. *Adv. Energy Mater.* **2017**, *7* (8), 1601488.

(8) Cao, J.; Tao, M.; Chen, H.; Xu, J.; Chen, Z. A highly reversible anthraquinone-based anolyte for alkaline aqueous redox flow batteries. *J. Power Sources* **2018**, *386*, 40.

(9) Kwabi, D. G.; Lin, K.; Ji, Y.; Kerr, E. F.; Goulet, M.-A.; De Porcellinis, D.; Tabor, D. P.; Pollack, D. A.; Aspuru-Guzik, A.; Gordon, R. G.; Aziz, M. J. Alkaline quinone flow battery with long lifetime at pH 12. *Joule* **2018**, *2*, 1907.

(10) Liu, T.; Wei, X.; Nie, Z.; Sprenkle, V.; Wang, W. A Total Organic Aqueous Redox Flow Battery Employing a Low Cost and Sustainable Methyl Viologen Anolyte and 4-HO-TEMPO Catholyte. *Adv. Energy Mater.* **2016**, *6* (3), 1501449.

(11) Janoschka, T.; Morgenstern, S.; Hiller, H.; Friebe, C.; Wolkersdorfer, K.; Häupler, B.; Hager, M. D.; Schubert, U. S. Synthesis and characterization of TEMPO- and viologen- polymers for water-based redox-flow batteries. *Polym. Chem.* **2015**, *6* (45), 7801.

(12) DeBruler, C.; Hu, B.; Moss, J.; Liu, X.; Luo, J.; Sun, Y.; Liu, T. L. Designer two-electron storage viologen anolyte materials for neutral aqueous organic redox flow batteries. *Chem.* **2017**, *3*, 961.

(13) Janoschka, T.; Martin, N.; Hager, M. D.; Schubert, U. S. An aqueous redox-flow battery with high capacity and power: the TEMPTMA/MV system. *Angew. Chem., Int. Ed.* **2016**, *55* (46), 14427.

(14) Beh, E. S.; De Porcellinis, D.; Gracia, R. L.; Xia, K. T.; Gordon, R. G.; Aziz, M. J. A neutral pH aqueous organic-organometallic redox flow battery with extremely high capacity retention. *ACS Energy Lett.* **2017**, *2* (3), 639.

(15) Hu, B.; DeBruler, C.; Rhodes, Z.; Liu, T. L. Long-cycling aqueous organic redox flow battery (AORFB) toward sustainable and safe energy storage. *J. Am. Chem. Soc.* **2017**, *139* (3), 1207.

(16) Lin, K.; Gómez-Bombarelli, R.; Beh, E. S.; Tong, L.; Chen, Q.; Valle, A.; Aspuru-Guzik, A.; Aziz, M. J.; Gordon, R. G. A redox-flow battery with an alloxazine-based organic electrolyte. *Nat. Energy* **2016**, *1* (9), 16102.

(17) Orita, A.; Verde, M. G.; Sakai, M.; Meng, Y. S. A biomimetic redox flow battery based on flavin mononucleotide. *Nat. Commun.* **2016**, *7*, 13230.

(18) Hollas, A.; Wei, X.; Murugesan, V.; Nie, Z.; Li, B.; Reed, D.; Liu, J.; Sprenkle, V.; Wang, W. A biomimetic high-capacity phenazine-based anolyte for aqueous organic redox flow batteries. *Nat. Energy* **2018**, *3* (6), 508.

(19) Winsberg, J.; Muench, S.; Hagemann, T.; Morgenstern, S.; Janoschka, T.; Billing, M.; Schacher, F. H.; Hauffman, G.; Gohy, J.-F.; Hoepfner, S.; Hager, M. D.; Schubert, U. S. Polymer/zinc hybrid-flow battery using block copolymer micelles featuring a TEMPO corona as catholyte. *Polym. Chem.* **2016**, *7* (9), 1711.

- (20) Dweck, A. C. Natural ingredients for colouring and styling. *Int. J. Cosmet. Sci.* **2002**, *24* (5), 287.
- (21) Wedege, K.; Drazevic, E.; Konya, D.; Bentien, A. Organic Redox Species in Aqueous Flow Batteries: Redox Potentials, Chemical Stability and Solubility. *Sci. Rep.* **2016**, *6*, 39101.
- (22) Hu, P.; Lan, H.; Wang, X.; Yang, Y.; Liu, X.; Wang, H.; Guo, L. Renewable-lawsone-based sustainable and high-voltage aqueous flow battery. *Energy Storage Mater.* **2019**, *19*, 62.
- (23) Hooper-Burkhardt, L.; Krishnamoorthy, S.; Yang, B.; Murali, A.; Nirmalchandar, A.; Prakash, G. K. S.; Narayanan, S. R. A New Michael-Reaction-Resistant Benzoquinone for Aqueous Organic Redox Flow Batteries. *J. Electrochem. Soc.* **2017**, *164* (4), A600.
- (24) Tabor, D. P.; Gómez-Bombarelli, R.; Tong, L.; Gordon, R. G.; Aziz, M. J.; Aspuru-Guzik, A. Mapping the frontiers of quinone stability in aqueous media: implications for organic aqueous redox flow batteries. *J. Mater. Chem. A* **2019**, *7* (20), 12833.
- (25) Wang, C.; Yang, Z.; Wang, Y.; Zhao, P.; Yan, W.; Zhu, G.; Ma, L.; Yu, B.; Wang, L.; Li, G.; Liu, J.; Jin, Z. High-Performance Alkaline Organic Redox Flow Batteries Based on 2-Hydroxy-3-carboxy-1,4-naphthoquinone. *ACS Energy Lett.* **2018**, *3* (10), 2404.
- (26) Miller-Chou, B. A.; Koenig, J. L. A review of polymer dissolution. *Prog. Polym. Sci.* **2003**, *28* (8), 1223.
- (27) Goulet, M.-A.; Tong, L.; Pollack, D. A.; Tabor, D. P.; Odom, S. A.; Aspuru-Guzik, A.; Kwan, E. E.; Gordon, R. G.; Aziz, M. J. Extending the Lifetime of Organic Flow Batteries via Redox State Management. *J. Am. Chem. Soc.* **2019**, *141* (20), 8014.
- (28) Badalyan, A.; Stahl, S. S. Cooperative electrocatalytic alcohol oxidation with electron-proton-transfer mediators. *Nature* **2016**, *535*, 406.
- (29) Weiss, C. J.; Wiedner, E. S.; Roberts, J. A. S.; Appel, A. M. Nickel phosphine catalysts with pendant amines for electrocatalytic oxidation of alcohols. *Chem. Commun.* **2015**, *51* (28), 6172.
- (30) Cheung, K.-C.; Wong, W.-L.; Ma, D.-L.; Lai, T.-S.; Wong, K.-Y. Transition metal complexes as electrocatalysts—Development and applications in electro-oxidation reactions. *Coord. Chem. Rev.* **2007**, *251* (17), 2367.
- (31) Francke, R.; Little, R. D. Redox catalysis in organic electrosynthesis: basic principles and recent developments. *Chem. Soc. Rev.* **2014**, *43* (8), 2492.
- (32) Bruce, D. B.; Thomson, R. H. 521. Aromatic keto-enols. Part II. Some new 2:3-dihydro-1:4-naphthoquinones and -anthraquinones. *J. Chem. Soc.* **1952**, 2759.
- (33) Thomson, R. H. 352. The structure of  $\beta$ -hydrojuglone and related compounds. Keto-enols of the naphthalene series. *J. Chem. Soc.* **1950**, 0, 1737.



**Molecular Engineering of an Alkaline Naphthoquinone Flow Battery**

*Liuchuan Tong, Marc-Antoni Goulet, Daniel P. Tabor, Emily F. Kerr, Diana De Porcellinis, Eric M. Fell, Alán Aspuru-Guzik, Roy G. Gordon,\* and Michael J. Aziz\**

Dr. Liuchuan Tong, Dr. Daniel P. Tabor, Dr. Alán Aspuru-Guzik, Dr. Roy G. Gordon  
Department of Chemistry and Chemical Biology, Harvard University, 12 Oxford Street,  
Cambridge, Massachusetts 02138, USA

Dr. Marc-Antoni Goulet, Dr. Diana De Porcellinis, Eric M. Fell, Dr. Michael J. Aziz  
Harvard John A. Paulson School of Engineering and Applied Sciences, 29 Oxford Street,  
Cambridge, Massachusetts 02138, USA

**Present Addresses**

Dr. Marc-Antoni Goulet

Form Energy Inc., Somerville, Massachusetts 02143, United States

Dr. Alán Aspuru-Guzik

Department of Chemistry and Department of Computer Science; Vector Institute for  
Artificial Intelligence, University of Toronto, Toronto, Ontario, M5S 1A1, Canada

\*Corresponding authors:

**Roy G. Gordon**

Cabot Professor

Dept. of Chemistry and Chemical Biology

Harvard University

12 Oxford Street, MA 02138, USA

Tel: +1 617-495-4017

Fax: +1 617-495-4723

email: Gordon@chemistry.harvard.edu

**Michael J. Aziz**

Gene and Tracy Sykes Professor of  
Materials and Energy Technologies

Harvard John A. Paulson School of  
Engineering and Applied Sciences, Pierce  
Hall 204a

29 Oxford Street, MA 02138, USA

Tel: +1 (617) 495-9884

email: maziz@harvard.edu

## Table of Contents

Synthesis of bislawsone .....	3
Electrochemical Characterization .....	3
Permeability Measurement.....	3
Full Cell Measurements .....	4
High-resolution LC-MS and preparative HPLC experiments.....	4
Theoretical Calculations.....	5
Figure S1 .....	6
Figure S2 .....	7
Figure S3 .....	8
Table S1 .....	8
Figure S4 .....	9
Figure S5 .....	10
Figure S6 .....	11
Figure S7 .....	12
Figure S8 .....	13
Figure S9 .....	14
Figure S10 .....	15
Figure S11 .....	17
Figure S12 .....	18
Figure S13 .....	19
Figure S14 .....	20
Figure S15 .....	21
Figure S16 .....	22
Table S2. ....	23
Frequently Asked Questions .....	26
References .....	26

## Synthesis of bislawsone

The synthesis was carried out according to literature<sup>1</sup> with modifications.

**Bislawsone, 2,2'-Bi(3-hydroxy-1,4-naphthoquinone).** 2-hydroxynaphthoquinone (6.35 g, 36.46 mmol) and ammonium persulfate (16.64 g, 72.92 mmol) were dissolved in 240 mL of acetonitrile and water mixture (1:1 v/v) and refluxed for three hours at 80 °C. 20 mL glacial acetic acid was added to the cooled mixture before filtration to obtain a yellow solid (5.68 g, 45% yield). Additional acetic acid wash may be employed if NMR of the product showed the presence of impurities. <sup>1</sup>H NMR (500 MHz, DMSO-d<sub>6</sub>): 8.10 (2H, d), 8.01 (2H, d), 7.86 (4H, m). <sup>13</sup>C NMR (125 MHz, DMSO-d<sub>6</sub>): 182.30, 180.19, 156.41, 134.96, 133.56, 132.06, 130.18, 126.13, 125.98, 115.50

## Electrochemical Characterization

### *Cyclic Voltammetry (CV) and Rotating Disk Electrode (RDE) Measurements*

Glassy carbon was used as the working electrode for all three-electrode CV tests. RDE experiments were conducted using a Pine Instruments Modulated Speed Rotator AFMSRCE equipped with a 5 mm diameter glassy carbon working electrode, a Ag/AgCl reference electrode (BASi, pre-soaked in 1 M KCl solution), and a graphite counter electrode. The electrode was rotated at a specific speed while the voltage was linearly swept from -0.4 to -1.4 V vs Ag/AgCl (a). The diffusion coefficient of the oxidized form of bislawsone was calculated using the Levich equation, which relates the mass transport-limited current to the number of electrons transferred ( $n$ ), the area of the electrode ( $A$ ), and the concentration of redox-active species in the electrolyte ( $C$ ), by plotting the mass-transport-limited current against the square root of the rotation rate (b), with the following parameters:  $n = 4$ ,  $F = 96,485$  Coulombs/mol,  $A = 0.196$  cm<sup>2</sup>,  $C = 5$  mM, kinematic viscosity of 1 M KOH,  $\nu = 1.08 \times 10^{-6}$  m<sup>2</sup>/s. The resulting value of the diffusion coefficient for the oxidized form of bislawsone is  $4.54 \times 10^{-6}$  cm<sup>2</sup>/s.

## Permeability Measurement

The permeability of the oxidized form of lawsone and bislawsone across a Fumasep E-620K membrane was evaluated with a lab-made two-compartment cell. The donating side was filled with a solution of lawsone or bislawsone (0.05 M) in 1 M KOH, while the receiving side was filled with 0.024 M KCl in 1 M KOH to balance the osmotic pressure. Both compartments had the same volume. The solutions were continuously mixed by keeping the cell on a rotating table. At different time intervals, aliquots were taken from the receiving side, diluted, characterized by UV-Vis spectrophotometry and replaced by fresh KOH solution. The concentration was calculated from a calibration curve and the permeability of lawsone and bislawsone was calculated based on Fick's law using the following equation:

$$P = \frac{\Delta \ln\left(1 - \frac{2c_t}{c_0}\right) \left(-\frac{V_o l}{2A}\right)}{\Delta t}$$

where  $P$  is permeability coefficient [cm<sup>2</sup>/s],  $A$  is the effective membrane area [cm<sup>2</sup>],  $t$  is elapsed time [s],  $c_t$  [mol/L] is the concentration of active species in the receiving side at time  $t$ ,  $V_o$  is the volume of the solution in either compartment (5 cm<sup>3</sup>),  $l$  is the thickness of the membrane

( $\sim 20 \mu\text{m}$ ),  $c_o$  is the concentration of lawsone or bislawsone in the donating side at time zero (0.05 mol/L), and  $\Delta$  represents a finite difference.

### Full Cell Measurements

Flow cells were constructed similar to a previous report.<sup>2-3</sup> Pyrosealed POCO graphite flow plates with serpentine flow patterns were used for both electrodes. Each electrode comprised a  $5 \text{ cm}^2$  geometric surface area covered by a stack of three or four sheets of Sigracet SGL 39AA porous carbon paper pre-baked in air overnight at  $400 \text{ }^\circ\text{C}$ . A Fumasep E-620K membrane served as the ion-selective membrane between the carbon electrodes. The electrolyte was pumped at  $60 \text{ mL/min}$  controlled by Cole-Parmer Masterflex L/S peristaltic pumps. All cells were run inside a nitrogen-filled glove bag, and cell polarization and charge-discharge cycling were performed using a Biologic VSP 300 potentiostat.

For low concentration (0.1 M) full cell measurement, the posolyte volume was 44 mL and its composition, when assembled, was 0.20 M potassium ferrocyanide, 0.02 M potassium ferricyanide and 1 M KOH. The negolyte was prepared by dissolving 0.1 M bislawsone in its oxidized form in 1.2 M KOH solution resulting in 8 mL 0.1 M bislawsone and 1.2 M  $\text{K}^+$  and 1 M  $\text{OH}^-$  electrolyte solution.

For high concentration (0.5 M) full cell measurement, the posolyte volume was 95 mL and its composition, when assembled, was 0.30 M potassium ferrocyanide, 0.10 M potassium ferricyanide and 1 M KOH. The negolyte was prepared by dissolving 0.5 M bislawsone in its fully oxidized form in 2.0 M KOH solution resulting in 8 mL 0.5 M bislawsone and 2 M  $\text{K}^+$  and 1 M  $\text{OH}^-$  electrolyte solution for Figure 3A, 3B, 3C, and 6 mL 0.5 M bislawsone and 2 M  $\text{K}^+$  and 1 M  $\text{OH}^-$  electrolyte solution for Figure 3D.

Galvanostatic cycling was performed at  $\pm 0.1 \text{ A/cm}^2$  at room temperature, with voltage limits and holds of 0.5 and 1.4 V until currents drop below  $2 \text{ mA/cm}^2$ . To obtain the polarization curves, the cell was first charged to the desired state of charge, and then polarized via linear sweep voltammetry at a rate of  $100 \text{ mV/s}$ . For high concentration 0.5 M bislawsone cell,  $\pm 0.3 \text{ A/cm}^2$  current was applied after the initial 12.6 days of cycling at  $\pm 0.1 \text{ A/cm}^2$ .

### High-resolution LC-MS and preparative HPLC experiments

High-resolution LC-MS analysis of electrolyte was performed in the Small Molecule Mass Spectrometry Facility at Harvard on a Bruker Impact II q-TOF with internal calibration sodium formate clusters. Liquid chromatography was performed on an Agilent 1290 Infinity HPLC using a Allure PFPP column ( $5 \mu\text{m}$  particle size,  $150 \times 2.1 \text{ mm}$ ) at a flow rate of  $0.4 \text{ mL/min}$  and the following elution conditions were applied (solvent A = 0.1% v/v formic acid in water; solvent B = 0.1% v/v formic acid in acetonitrile): 95% solvent A for 2 min, a gradient increasing from 5% to 60% solvent B in solvent A over 13 min, a gradient increasing to 100% solvent B over 5 min, a gradient decreasing to 5% solvent B in solvent A over 0.1 min, and 100% solvent A for 4.9 min. The ESI mass spectra were recorded in negative ionization mode.

Preparative HPLC was performed using a Thermo Scientific Hypersil GOLD aQ column ( $5 \mu\text{m}$  particle size,  $250 \times 20 \text{ mm}$ ) at a flow rate of  $10 \text{ mL/min}$  and the following elution conditions were applied (solvent A = 0.1% v/v formic acid in water; solvent B = 0.1% v/v formic acid in acetonitrile): 80% solvent A for 2 min, a gradient increasing from 20% to 70% solvent B in



solvent A over 5 min, a gradient increasing to 85% solvent B over 10 min, a gradient increasing to 95% solvent B over 4 min, a gradient decreasing to 20% solvent B in solvent A over 1 min, and 20% solvent B for 2 min. The eluent fractions were collected and lyophilized for subsequent LC-MS confirmation

### Theoretical Calculations

We calculated the properties of a library of lawsone-derived molecules in order to gain some understanding for the increased stability of bislawsone relative to lawsone and identify candidates that may have superior performance to bislawsone. The results of the full library are provided in the supplementary spreadsheet. The primary modifications include varying the number of carbon atoms between the lawsone units and the functional groups attached to the benzene ring. Functional groups considered include hydroxyl, methoxy, ethoxy, methyl, ethyl, CH<sub>2</sub>-CH<sub>2</sub>-OH, amine, and the oxy-butyrate functional group (with the number of carbons varied) employed in 2-6 DBEAQ.

For the calculations, the molecules are left in their neutral forms to reduce errors associated with calculating the energies of anions. This leads to a slightly overestimation of the reduction potentials, but the overestimation is mostly systematic and by looking at differences we can capture all of the relevant structure-property relationships. Energetics are evaluated at the B3LYP/6-311+G(d,p) (PCM) level of theory.

The calculated thermodynamic susceptibility of the reduced forms of bislawsone tautomerizing to the partially redox inactive forms is shown in Figure 4A. These calculated reaction energies are over 0.1 eV higher than the analogous tautomerization energy for lawsone (0.02 eV), indicating that forming this dimer mitigates the effects of this decomposition mechanism. The calculations also predict that the half-reduced (2e<sup>-</sup> reduced) form is more susceptible to tautomerization than the fully reduced form (4e<sup>-</sup> reduced).

Within the set of 193 bislawsone derivatives, we found 8 derivatives that are predicted to be more stable than bislawsone (against both “type 1” and “type 2” decomposition) and have reduction potentials within 0.1V of bislawsone. This set of molecules is shown in Figure S16. Examining these molecules, we see a variety of viable derivatives that vary the number of carbon atoms between the lawsone subunits (up to 3) but see a common pattern in the functional groups that are predicted to increase stability. These alkyl groups terminated by an alkoxy group on one end and a carboxylic acid group are emerging as common motifs in stabilized anthraquinone flow battery molecules. One molecule, with a two-carbon linkage between the lawsone units, and 4 total functionalizations (of the -OCCCCOOH type) is predicted to be both more stable and lower in reduction potential (by about 0.04 V) than bislawsone.

Figure S1

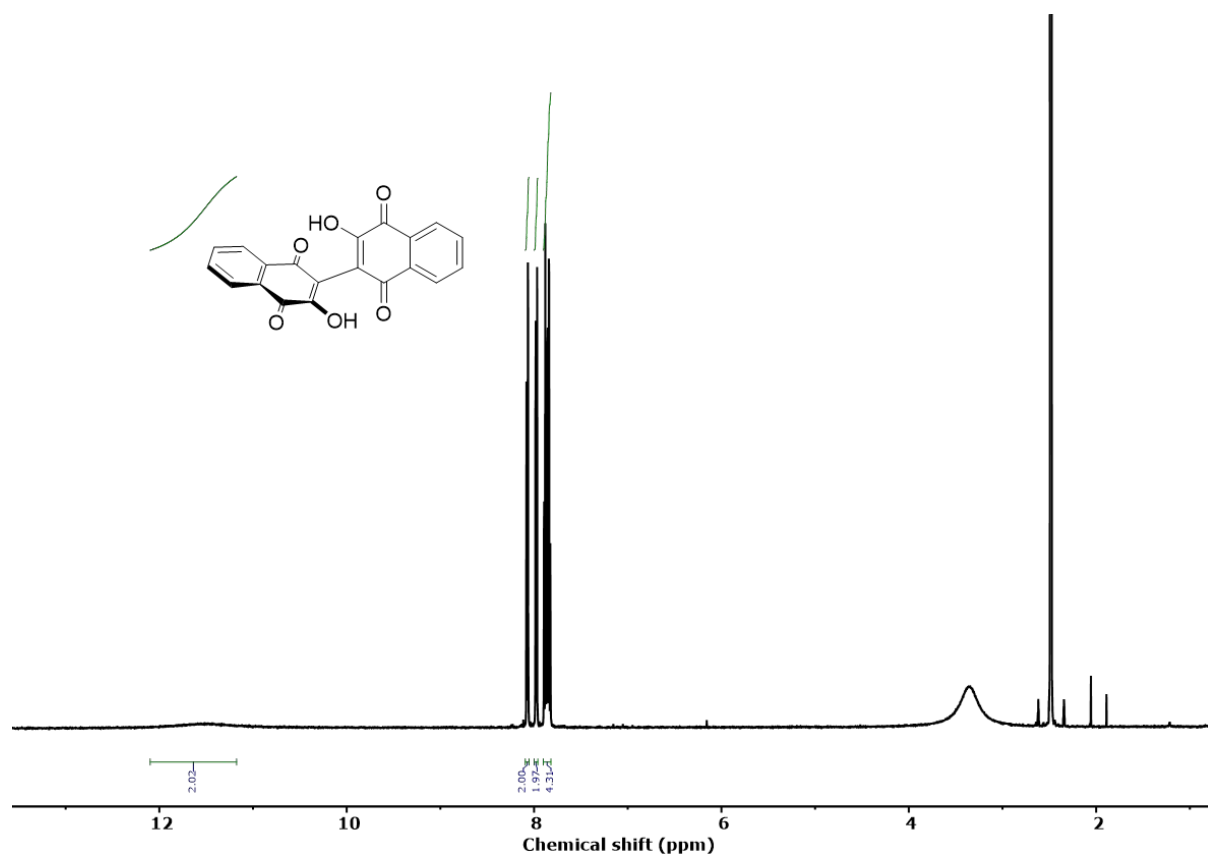


Figure S1 <sup>1</sup>H NMR spectrum of bislawsone in DMSO-d<sub>6</sub>. <sup>1</sup>H NMR (500 MHz, DMSO-d<sub>6</sub>) δ: 11.51 (br, 2H), 8.07 (d, 2H), 7.97 (dd, 2H), 7.90-7.82 (m, 4H).

Figure S2

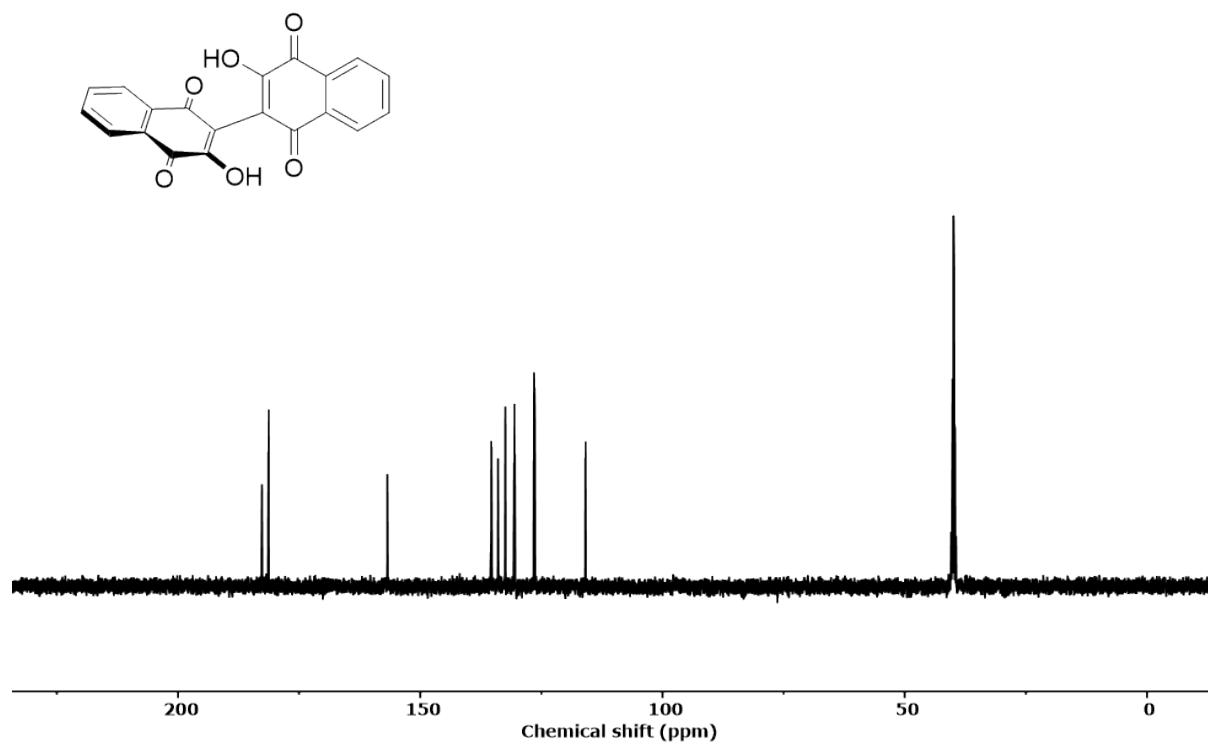


Figure S2  $^{13}\text{C}$  NMR spectrum of bislawsone in DMSO- $d_6$ .  $^{13}\text{C}$  NMR (125 MHz,  $\text{CDCl}_3$ )  $\delta$ : 182.68, 181.29, 156.79, 135.33, 133.94, 133.44, 130.56, 126.51, 126.36, 115.89.

**Figure S3**

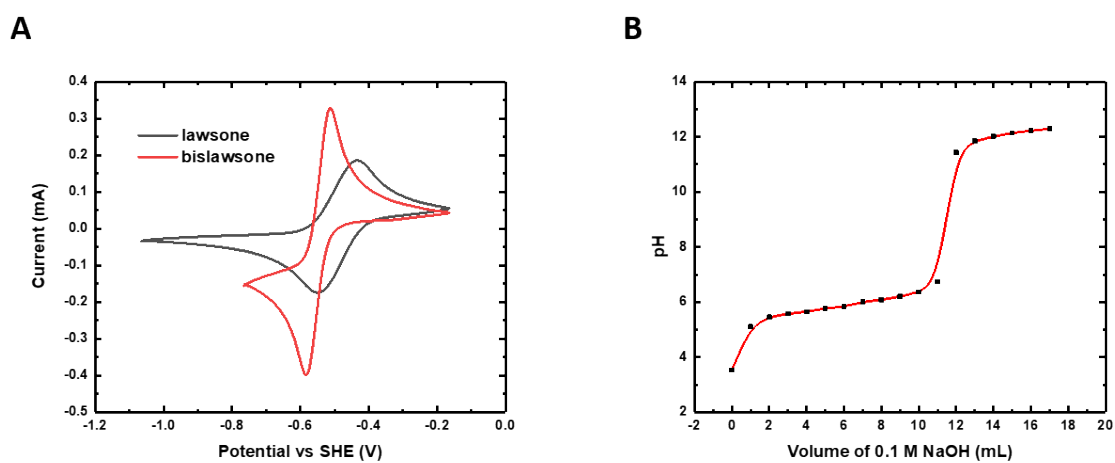


Figure S3. (A) Cyclic voltammograms of 5 mM bislawsone (red), and 5 mM lawsone (black) in 1M KOH at a scan rate of 50 mV/s. (B) Titration of 10 mL 0.1M lawsone with 0.1 M NaOH solution

**Table S1** Comparison of bislawsone with lawsone.

	Reduction potential (vs SHE in 1M KOH)	Solubility	pKa	Permeability
lawsone	-0.501 V	0.48 M	6.0	$1.01 \times 10^{-10} \text{ cm}^2/\text{s}$
bislawsone	-0.551 V	0.56 M	6.5	$1.19 \times 10^{-11} \text{ cm}^2/\text{s}$



Figure S4

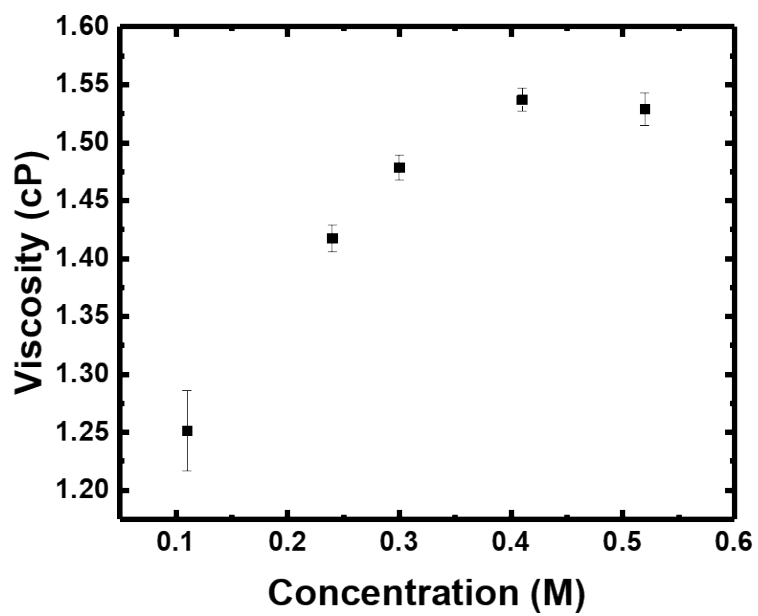


Figure S4. Viscosity measurement of bislawson at various concentration in 1M KOH

Figure S5

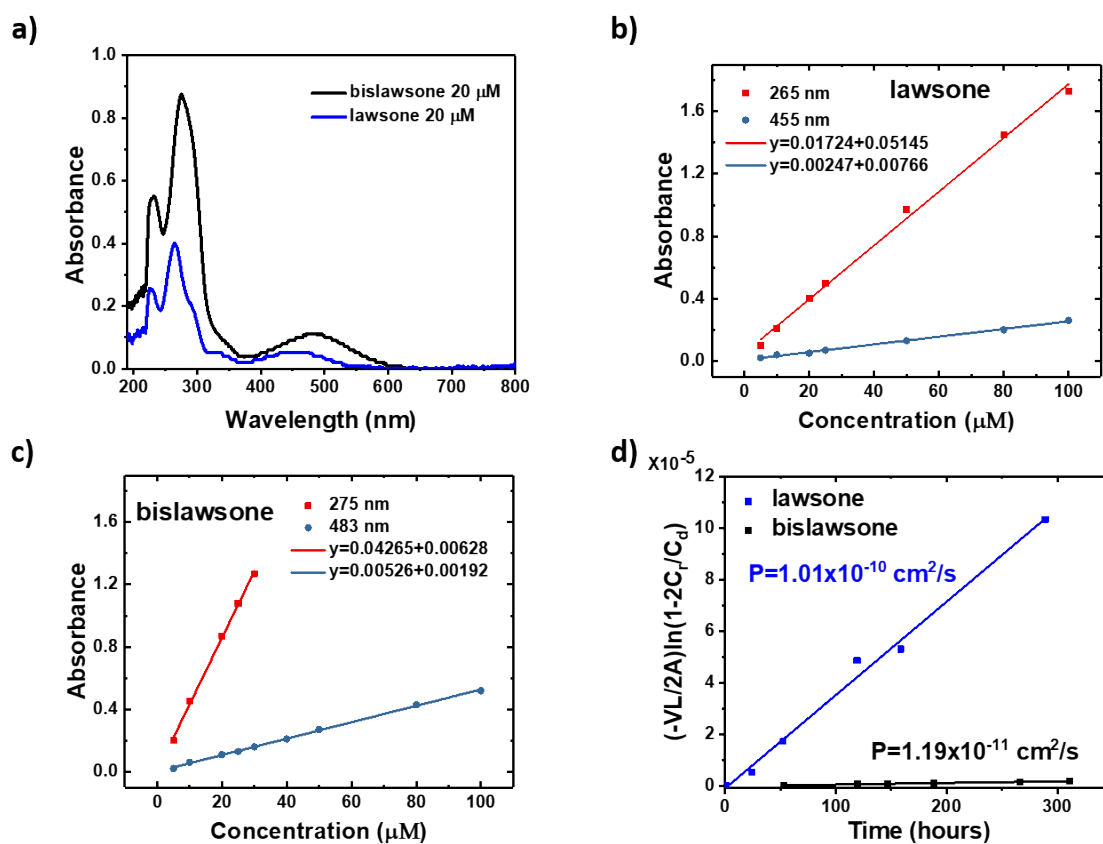


Figure S5. (a) Representative UV-Vis spectrum of lawsone and bislawsone at 20  $\mu\text{M}$  in 1M KOH. (b) Calibration curve of lawsone in 1 M KOH. Peaks at 265 and 455 nm were selected for calibration. (c) Calibration curve of bislawsone in 1 M KOH. Peaks at 275 and 483 nm were selected for calibration. (d) Comparison of permeability of lawsone and bislawsone in 1 M KOH through Fumasep E-620K based on crossover test.

Figure S6

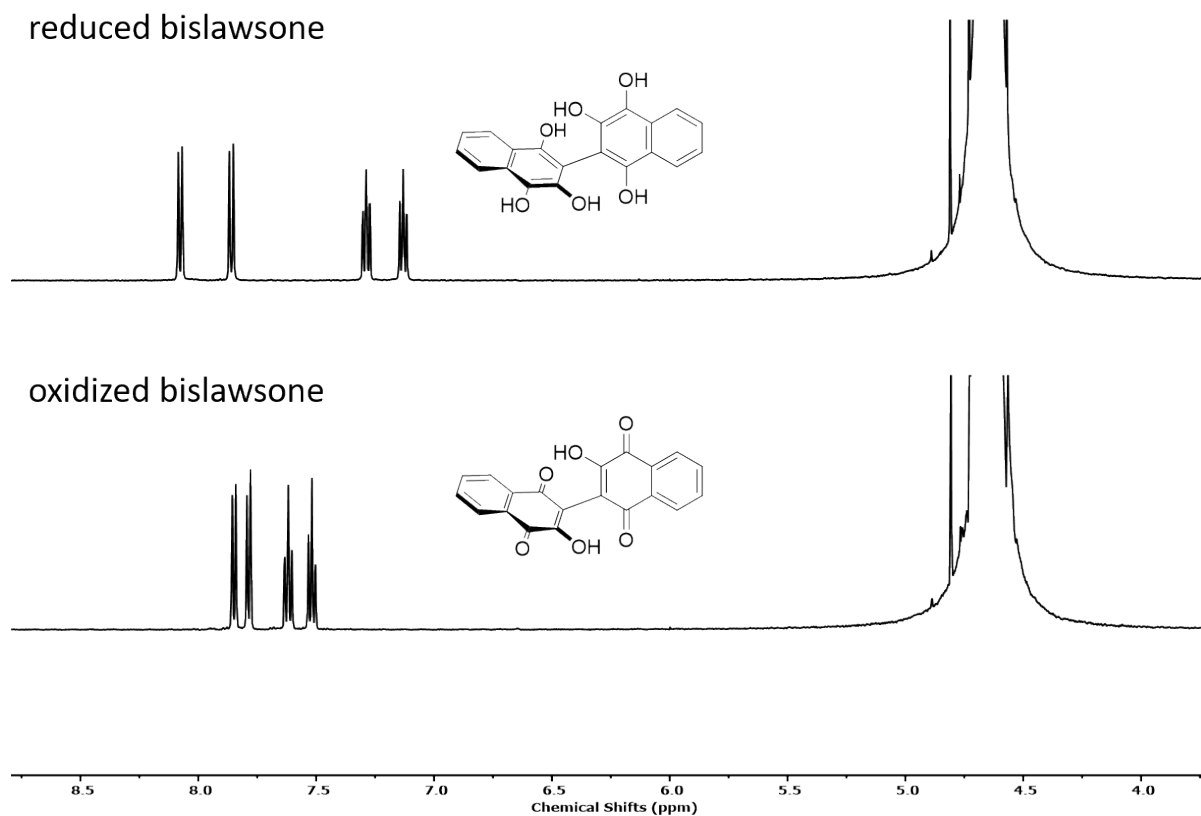


Figure S6  $^1\text{H}$  NMR spectrum of fully reduced bislawsone (top) and oxidized bislawsone (bottom) in  $\text{D}_2\text{O}/\text{KOH}$  solution after 3 cycles. Reduced bislawsone:  $^1\text{H}$  NMR (500 MHz,  $\text{CDCl}_3$ )  $\delta$ : 8.07 (d, 2H), 7.86 (d, 2H), 7.28 (dd, 2H), 7.13 (dd, 2H). Oxidized bislawsone:  $^1\text{H}$  NMR (500 MHz,  $\text{CDCl}_3$ )  $\delta$ : 7.85 (d, 2H), 7.78 (d, 2H), 7.62 (dd, 2H), 7.52 (dd, 2H).

Figure S7

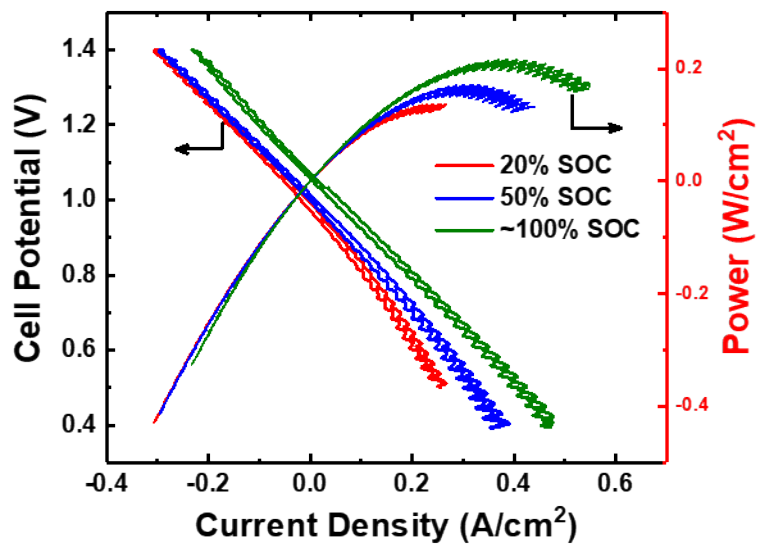


Figure S7 Electrochemical performance of a 0.1 M bislawsonone/ $K_4Fe(CN)_6$  cell. The cell-polarization plots, composed of cell potential (left vertical) and power density (right vertical) versus current density.



Figure S8

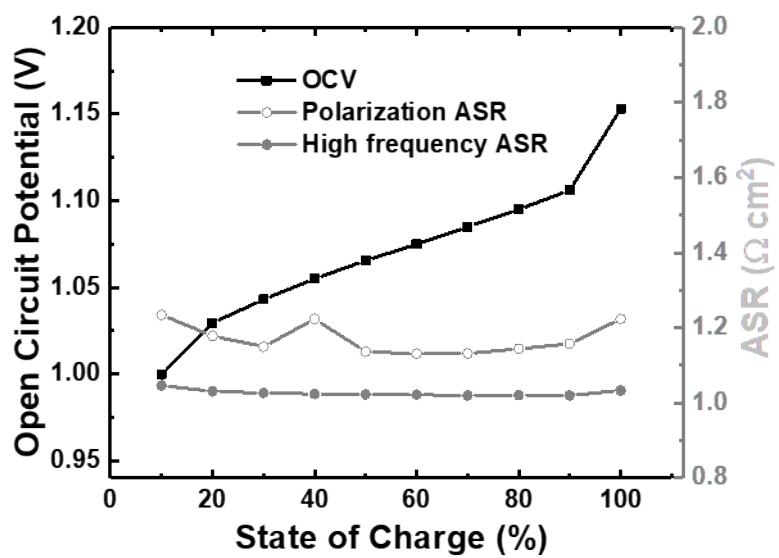


Figure S8. OCV, high-frequency, and polarization ASR versus SOC of 0.5 M bislawsone cell

Figure S9

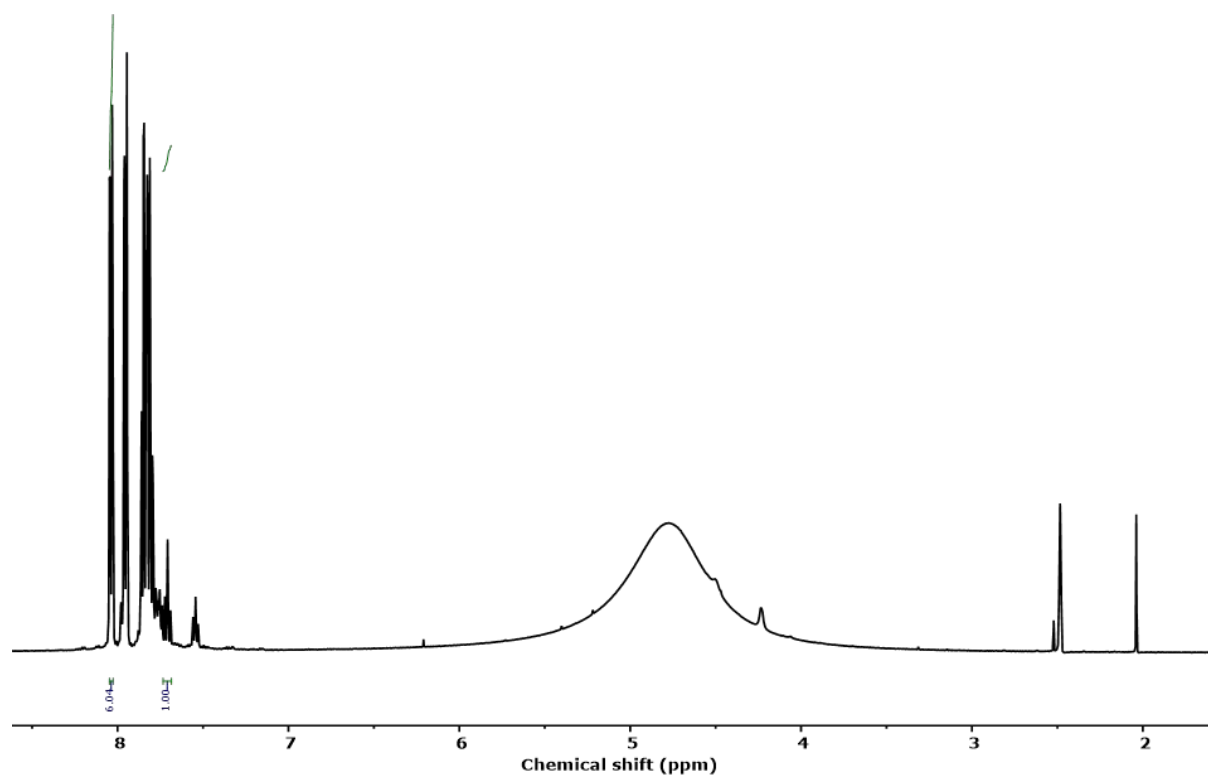


Figure S9. NMR spectrum of cyclized bislowsone in DMSO after acidified with HCl.

Figure S10

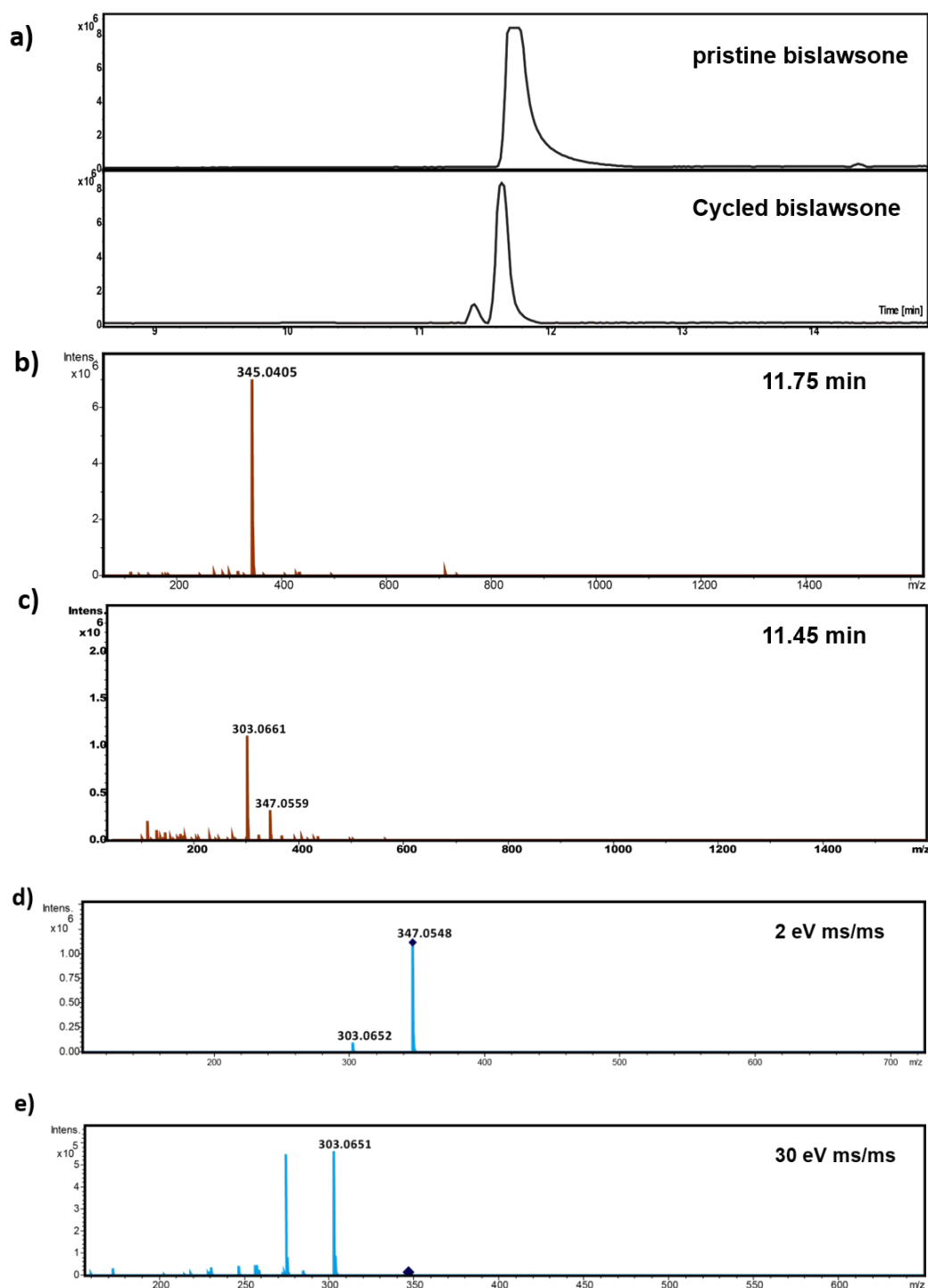
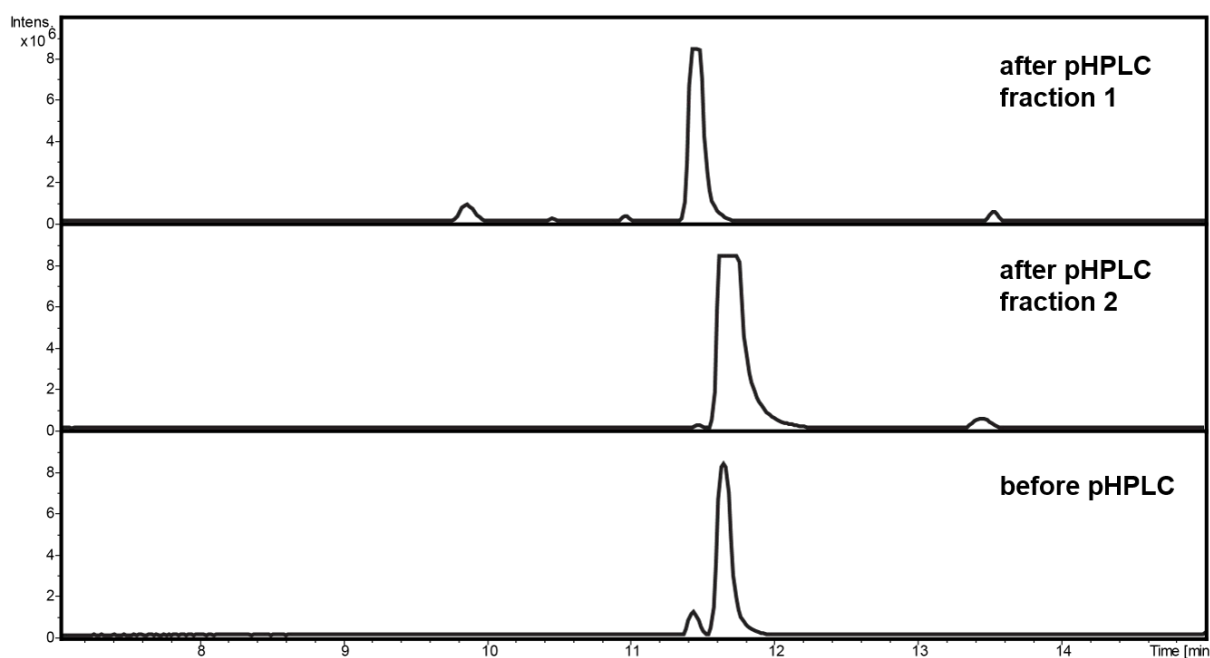


Figure S10 **High-resolution liquid chromatograph mass spectrometry.** (a) LC-MS of pristine bislawsone (top) and a bislawsone sample that has been cycled for 21 days (bottom). (b) Mass spectrum of cycled sample at 11.75 min showing the major peak is bislawsone ( $m/z = 345.0405$ ). (c) Mass spectrum of cycled sample at 11.45 min showing the degradation product  $m/z$  of 347.0559, and fragment  $m/z$  of 303.0661. (d) Tandem LC-MSMS of  $m/z$  347.0548 at minimal 2 eV shows that minimal fragmentation occurred. (e) Tandem LC-MSMS of  $m/z$  347.0548 at high 30 eV shows that most of the parent ion fragmented into  $m/z = 303.0651$ . This result confirms that  $m/z = 303.0651$  signal is a fragment of parent  $m/z = 347.0548$  instead

of an independent species that is coeluting. The diamond symbol indicates the target mass for fragmentation.



**Figure S11**



**Figure S11. LC-MS of Fractions Collected from Preparative High-Performance Liquid Chromatography Separation** LC-MS traces showing cycled bislawone mixture before pHPLC separation(bottom), purified bislawone fraction at 11.75 min (middle), and purified degradation product at 11.45 min. This result showed that the degradation product can be purified from cycled electrolyte mixture for structure identification. The small peaks at 10 min and 13.5 min are impurities from pHPLC columns and do not affect subsequent NMR analysis.

Figure S12

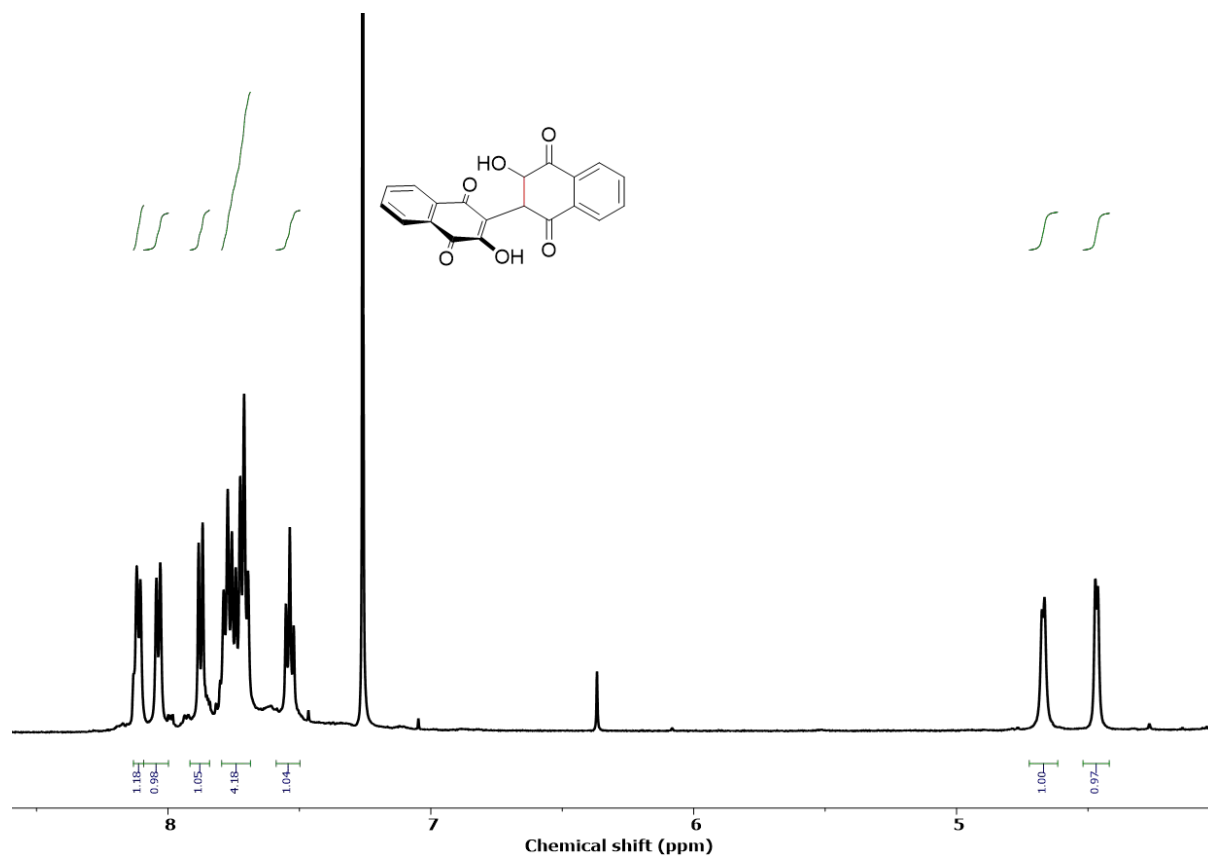


Figure S12. **<sup>1</sup>H NMR spectrum of degradation product 2,3-dihydrobislawsonone.** <sup>1</sup>H NMR (500 MHz, CDCl<sub>3</sub>) δ: 8.12 (d, 1H), 8.04 (d, 1H), 7.88 (d, 1H), 7.80-7.68 (m, 4H), 7.54 (dd, 1H), 4.67 (d, 1H), 4.47 (d, 1H). The presence of inter-splitting aliphatic proton indicates the presence of carbon-carbon single bond.

Figure S13

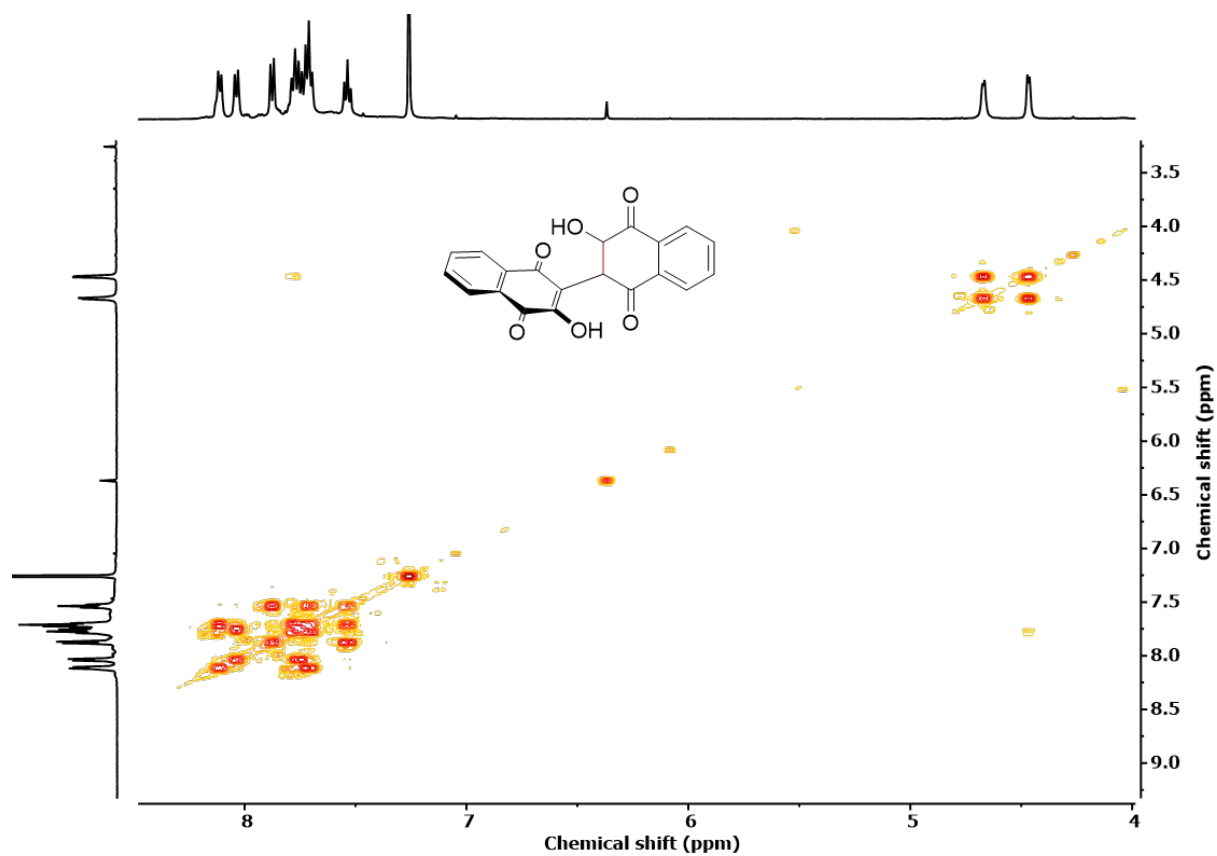


Figure S13. COSY NMR spectrum of degradation product 2,3-dihydrobislawsonic acid. Two aliphatic protons split each other.

Figure S14

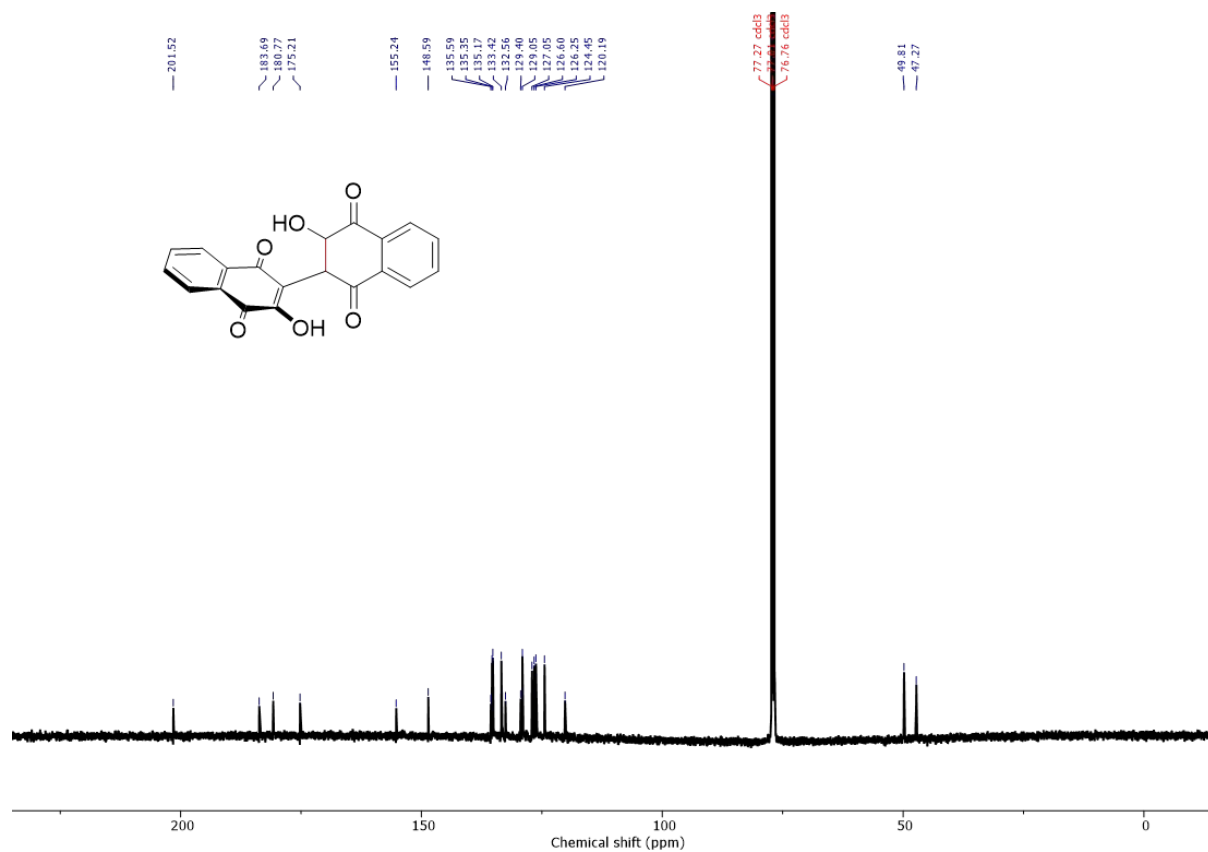


Figure S14.  $^{13}\text{C}$  NMR spectrum of degradation product **2,3-dihydrobislawsonine**.  $^{13}\text{C}$  NMR (125 MHz,  $\text{CDCl}_3$ )  $\delta$ : 201.5, 183.69, 180.77, 175.21, 155.24, 148.59, 135.59, 135.35, 135.17, 133.42, 132.56, 129.40, 129.05, 127.05, 126.60, 126.25, 124.45, 120.19, 49.81, 47.27. A total of 20 distinct carbon peaks indicate the asymmetry of the structure.

Figure S15

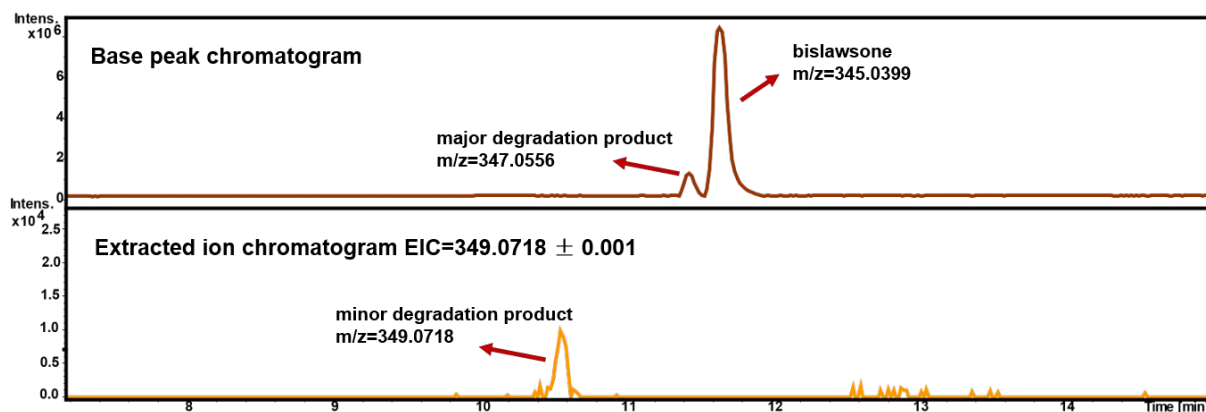


Figure S15. LC-MS detection of redox-inactive 2,2',3,3'-tetrahydrobislawsone. Top) Base peak chromatogram of 0.5 M bislawsone cell cycled for 21 days showing bislawsone peak at 11.7 min and 2,3-dihydrobislawsone peak as major degradation product at 11.4 min. Bottom) Extracted ion chromatogram of 349.0718 ± 0.001 showing the minor degradation product in around 1% concentration.



**Figure S16**

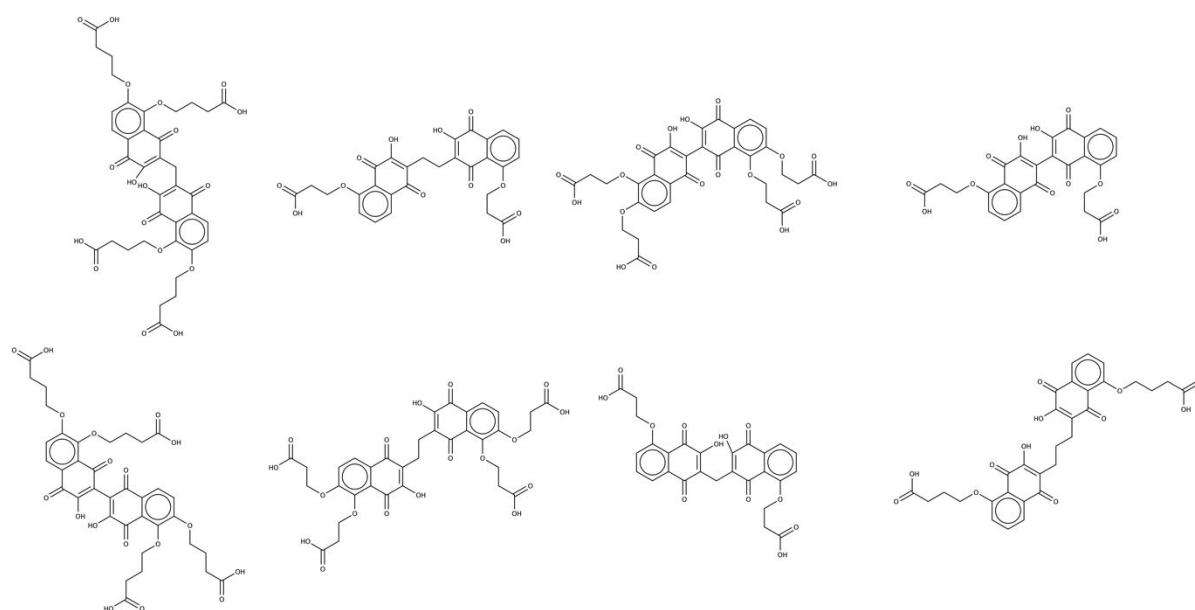
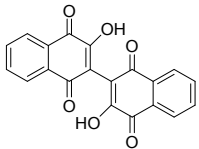
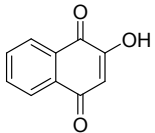
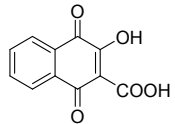
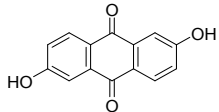
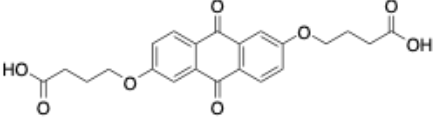
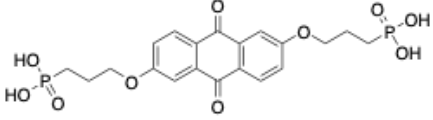
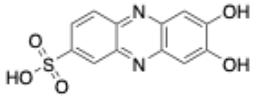
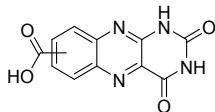
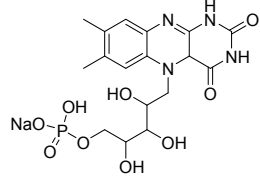
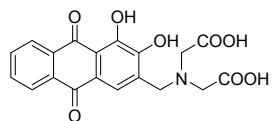


Figure S16. Predicted Stable Molecules. These molecules are bislawsone derivatives that are predicted to have two-proton-two-electron reduction within 0.1 V of bislawsone for each of the reduction reactions and are less thermodynamically susceptible to tautomerization than bislawsone. All energies (B3LYP/6-311+G(d,p) PCM) are provided in supplementary spreadsheet.

**Table S2.** Overview of reported high performance negolytes for alkaline organic flow battery (at pH 14 unless otherwise noted).

Negative electrolyte	Potential (V vs.SHE)	Solubility	# of electrons	Capacity loss per day
 Bislawsone (This work)	-0.55	0.56 M	4	0.75%
 2-hydroxy-1,4-naphthoquinone (lawsone) <sup>4</sup>	-0.49	0.48 M	2	4.1%
 2-hydroxy-3-carboxyl-1,4-naphthoquinone (2,3-HCNQ) <sup>4</sup>	-0.52	1.2 M	2	6.4%
 2,6-dihydroxyanthraquinone (DHAQ) <sup>3</sup>	-0.68	0.6 M	2	est. 5.6%.

 <p>2,6-DBEAQ<sup>2</sup></p>	-0.52	1.1M 0.6M (pH 12)	2	0.04% (pH 12)
 <p>2,6-DPPEAQ<sup>5</sup></p>	-0.47 (pH 9)	0.75M (pH 9)	2	0.014% (pH 9 - 12)
 <p>7,8-dihydroxyphenazine-2-sulfonic acid (DHPS)<sup>6</sup></p>	-0.85	1.8M	2	0.68%
 <p>alloxazine 7/8-carboxylic acid (ACA)<sup>7</sup></p>	-0.62	0.5 M	2	est. 0.93%
 <p>riboflavin-5'-monophosphate sodium salt (FMN-Na)<sup>8</sup></p>	-0.52	0.24 M	2	0.52%



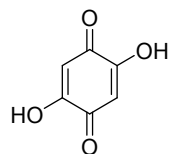
alizarin-3-methyliminodiacetic acid  
(AMA)<sup>9</sup>

-0.67

0.4 M

2

19.4%



2,6-dihydroxybenzoquinone  
(DHBQ)<sup>10</sup>

-0.72

4.31 M

2

est.9%

## Frequently Asked Questions

**Q:** Why was the Pourbaix diagram not measured?

**A:** We agree that the Pourbaix diagram offers insight into the proton and electron transfer processes of a redox system. However, bislawsone did not show a reversible CV signal in buffered solution from pH 12 to pH 2. The lack of reversible CV signal has also been observed in other alpha-hydroxy quinone systems 2,6-DihydroxyBenzoquinone (*Adv. Energy Mater.* 2018, **8**, 1702056). The exact origin of this phenomenon is unknown at this time.

**Q:** The initial Coulombic efficiency in Figure 2D is ~99%, but it rapidly increases to 99.5% at the time of 0.5 day. Why?

**A:** The cell was cycled in a nitrogen filled glovebag along with several other cells running in parallel in adjacent glovebags with the same nitrogen supply. The initial gradual increase in the Coulombic efficiency is due to a gradual depletion of dissolved oxygen gas in the electrolytes/cells which were prepared outside of the glove bag. The artifact of the ~0.5% jump in Coulombic efficiency at 0.5 day is most likely due to a sudden ramp in the nitrogen pressure or a better seal of the glove bag. Because the organic redox materials are sensitive to oxygen, we have observed this fluctuation in Coulombic efficiency in several cases where the nitrogen pressure was changed or a pinhole was created/sealed in the glovebag.

## References

1. Inagaki, R.; Ninomiya, M.; Tanaka, K.; Koketsu, M., Synthesis, Characterization, and Antileukemic Properties of Naphthoquinone Derivatives of Lawsone. *ChemMedChem* **2015**, *10* (8), 1413-1423.
2. Kwabi, D. G.; Lin, K.; Ji, Y.; Kerr, E. F.; Goulet, M.-A.; De Porcellinis, D.; Tabor, D. P.; Pollack, D. A.; Aspuru-Guzik, A.; Gordon, R. G.; Aziz, M. J., Alkaline quinone flow battery with long lifetime at pH 12. *Joule* **2018**, *2*, 1907.
3. Lin, K.; Chen, Q.; Gerhardt, M. R.; Tong, L.; Kim, S. B.; Eisenach, L.; Valle, A. W.; Hardee, D.; Gordon, R. G.; Aziz, M. J.; Marshak, M. P., Alkaline quinone flow battery. *Science* **2015**, *349* (6255), 1529-32.

4. Wang, C.; Yang, Z.; Wang, Y.; Zhao, P.; Yan, W.; Zhu, G.; Ma, L.; Yu, B.; Wang, L.; Li, G.; Liu, J.; Jin, Z., High-Performance Alkaline Organic Redox Flow Batteries Based on 2-Hydroxy-3-carboxy-1,4-naphthoquinone. *ACS Energy Letters* **2018**, *3* (10), 2404-2409.
5. Ji, Y.; Goulet, M.-A.; Pollack, D. A.; Kwabi, D. G.; Jin, S.; De Porcellinis, D.; Kerr, E. F.; Gordon, R. G.; Aziz, M. J., A Phosphonate-Functionalized Quinone Redox Flow Battery at Near-Neutral pH with Record Capacity Retention Rate. *Advanced Energy Materials* **2019**, *9* (12), 1900039.
6. Hollas, A.; Wei, X.; Murugesan, V.; Nie, Z.; Li, B.; Reed, D.; Liu, J.; Sprenkle, V.; Wang, W., A biomimetic high-capacity phenazine-based anolyte for aqueous organic redox flow batteries. *Nature Energy* **2018**, *3* (6), 508-514.
7. Lin, K.; Gómez-Bombarelli, R.; Beh, E. S.; Tong, L.; Chen, Q.; Valle, A.; Aspuru-Guzik, A.; Aziz, M. J.; Gordon, R. G., A redox-flow battery with an alloxazine-based organic electrolyte. *Nature Energy* **2016**, *1*, 16102.
8. Orita, A.; Verde, M. G.; Sakai, M.; Meng, Y. S., A biomimetic redox flow battery based on flavin mononucleotide. *Nat Commun* **2016**, *7*, 13230.
9. Liu, Y.; Lu, S.; Chen, S.; Wang, H.; Zhang, J.; Xiang, Y., A Sustainable Redox Flow Battery with Alizarin-Based Aqueous Organic Electrolyte. *ACS Applied Energy Materials* **2019**, *2* (4), 2469-2474.
10. Yang, Z.; Tong, L.; Tabor, D. P.; Beh, E. S.; Goulet, M.-A.; De Porcellinis, D.; Aspuru-Guzik, A.; Gordon, R. G.; Aziz, M. J., Alkaline Benzoquinone Aqueous Flow Battery for Large-Scale Storage of Electrical Energy. *Advanced Energy Materials* **2018**, *8* (8), 1702056.